A REVIEW OF AERONAUTICAL FATIGUE AND STRUCTURAL INTEGRITY IN ISRAEL
(2017 –2019)

Compiled by:
Dr. Yuval Freed
Engineering Division
Israel Aerospace Industries
***Ben-Gurion Airport*, Israel**
yfreed@iai.co.il

Presented at the 36th Conference of the International Committee on Aeronautical Fatigue and Structural Integrity (ICAF)
Krakow, Poland
3-4 June 2019

A REVIEW OF AERONAUTICAL FATIGUE AND STRUCTURAL INTEGRITY IN ISRAEL

JANUARY 2017 – DECEMBER 2018

SUMMARY

This review summarizes fatigue, structural-integrity and fracture-mechanics investigations that were performed in Israel during the period of January 2017 to December 2018. The review includes contributions from Israel Aerospace Industries Ltd. (IAI), Israel Air Force (IAF), Tel-Aviv University (TAU), Ben-Gurion University (BGU), RAFAEL and private consultants.

Presented at the 36th ICAF Conference
Krakow, Poland
3-4 June 2019

TABLE OF CONTENTS

A REVIEW OF AERONAUTICAL FATIGUE INVESTIGATIONS IN ISRAEL JANUARY 2017 – DECEMBER 2018

1. INTRODUCTION

The Israel National Review summarizes activities performed in the field of aeronautical fatigue, structural integrity, health monitoring and fracture mechanics in Israel during the period of January 2017 to December 2018. The previous National Review [1] covered activities up to the end of 2016. The following organizations contributed to this review:

- Israel Aerospace Industries Ltd. (IAI)
- Israel Air Force (IAF)
- Tel-Aviv University (TAU)
- Ben-Gurion University (BGU)
- RAFAEL
- Abraham Brot – Brot Engineering Consultant

The National Review was compiled by Dr. Yuval Freed (yfreed@iai.co.il).

2. FATIGUE ANALYSIS, TESTING AND LIFE EXTENSION

2.1 A Summary of New IAI Executive Jet Teardown Inspection (Y. Buimovich, Y. Freed, G. Noivirt and C. Matias, IAI)

Israel Aerospace Industries and another aerospace company have jointly developed a new super mid-size executive jet. The aircraft has a range of 3,400 nautical miles at a maximum speed of Mach 0.85. It can cruise at altitudes up to 45,000 feet. Its first flight took place during December 2009. Certification to the FAA, EASA, CAAI and TCCA regulations were completed, and type-certificates were obtained. Deliveries began in 2012.

The aircraft is powered by twin Honeywell HTF7250G engines, each producing 7,445 pounds of thrust. The aircraft is capable of nonstop flight from New York to London or from London to Dubai. The aircraft has a very roomy and quiet cabin. The cabin environment includes 100% fresh air and a cabin altitude not exceeding 7,000 feet. Its Design Life Goal (DLG) is 20,000 flights or 36,000 flight-hours.

As part of its damage-tolerance certification program, a structurally complete airframe test-article was fatigue tested for two lifetimes (40,000 flights), followed by half a lifetime (10,000 flights) of damage-tolerance testing with artificial flaws inflicted at selected critical locations. Residual strength tests, under limit loads and cabin pressurization, were performed in the presence of large cracks at several critical locations. This was reported in the 2017 National Review [1].

The teardown inspection is currently in progress. The preparations for the teardown inspection are shown in Figure 1.

Figure 1. Preparation for teardown inspection

2.2 Conversion of 737-700 Passenger to Freighter Aircraft (Y. Freed, IAI)

Israel Aerospace Industries has developed and certified in the past two decades converted freighter for a series of Boeing models, such as 747-200/400, 767-200/300 and 737-300/400. Its newest converted freighter, for Boeing 737-700 aircraft, was certified as a supplemental type certificate to the CAAI, FAA and EASA in September, 2017. The conversion includes the installation of a cargo door on the fuselage, additional structural modification to support full load capacity, and implementation of smoke and fire detection in the cargo bay. A solid 9g barrier/smoke partition is installed at aircraft forward fuselage, separating the class E compartment from the occupied area and creating a supernumeraries compartment in the area between the flight deck and the 9g barrier. Interiors, ECS, smoke detection, oxygen, lighting and other systems are modified to accommodate the freighter configuration. The converted B737-700BDSF can carry a total of 10 ULDs – eight full 88”×125” AAA plus one 80”×43” AYK plus one 88”×79” AYF, providing a total useful volume of 3,673 cu. ft., enabling it to carry up to 45,000 lb. An overview of the modifications in the 737-700BDSF aircraft is shown in Figure 2.

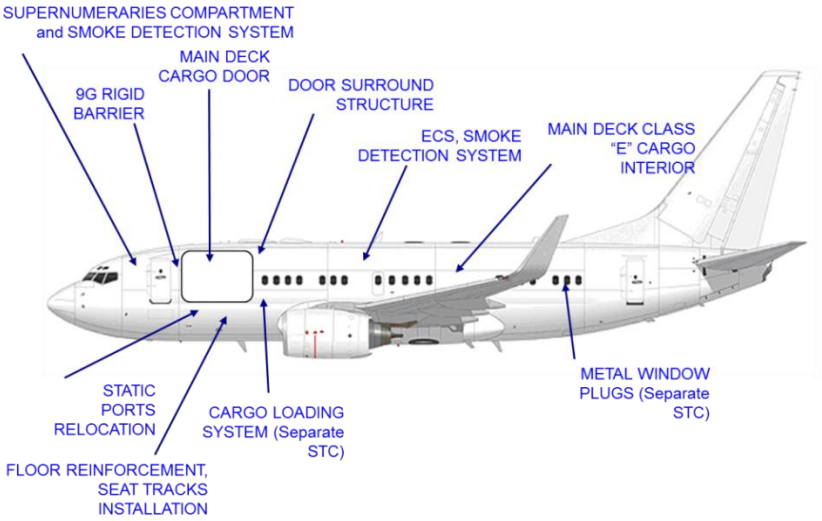

Figure 2. Modification at the 737-700BDSF aircraft

The modifications at the aircraft structure include:

- Installation of a Main Deck door surround structure
- Modification of left wing illumination light
- Installation of a Main Deck Cargo Door (MDCD)
- Installation of 9g Rigid Barrier
- Sliding door
- Incorporation of floor beam inspection access
- Installation of three new seat tracks
- Floor beams reinforcements
- Frames reinforcements
- Modification of floor panels
- Installation of Cargo Loading System
- Entry Door deactivation
- Installation of window plugs

Full structural substantiation was conducted to the airframe installations and modifications, as well as full aircraft assessment. The fatigue and damage tolerance substantiation program includes modified inspections to Boeing fatigue critical baseline structure inspections, as well as supplemental inspections to the fatigue critical alteration structure as well as the interface

elements between IAI and Boeing structures. The converted 737-700BDSF prototype is shown in Figure 3.

Figure 3. Converted 737-700BDSF aircraft during flight.

2.3 The dual threat of Sudden Decompression (A. Brot, Brot Engineering Consultant)

Sudden decompression can be a very dangerous incident for a commercial aircraft. Major structural damage to the fuselage, which compromises the structural-integrity of the aircraft, is often the cause of the sudden decompression. This process is often classified as Widespread Fatigue Damage (WFD).

An example of WFD is the loss of two Comet-1 aircraft in 1954. On the other hand, the sudden decompression could cause passengers and flight crew to lose consciousness, due to a lack of oxygen at high altitudes. An example of this is the sudden decompression of Southwest airlines flight 812 in 2011, where a flight attendant and a passenger briefly lost consciousness, until the aircraft descended to a lower altitude. If both pilots had lost consciousness, the aircraft might continue to fly at the high altitude until the aircraft expended all its fuel, resulting in a crash. This type of scenario resulted in a crash of a Learjet-35 in 1999.

Eleven instances of sudden decompression of airliners since 1994 have been compiled. Six of these were classified as "externally driven", and were not considered in this study. The remaining five instances were classified as "fatigue driven", and became part of this study. Table 1 presents a summary of these incidents.

Table 1. Eleven incidents of sudden decompression of a commercial airliner during flight

Year	Aircraft	Manufacturer	Airline	Flights at Failure	Number of Fatalities	Principal Cause of Failure
1954	Comet 1	de Havilland	BOAC	1,286	35	Fuselage frames lacked the ability to perform crack arrest.
1954	Comet 1	de Havilland	South African Airways	903	21	
1981	737-200	Boeing	Far Eastern Transport (Taiwan)	33,313	110	Extreme intergranular and exfoliation corrosion. Inspection was not performed properly.
1985	747-100 SP	Boeing	Japan Airlines	18,835	520	Improper repair of pressure dome.
1988	737-200	Boeing	Aloha Airlines	89,680	1	MSD cracking resulting from poor manufacturing processes.
1988	727-25	Boeing	Eastern Airlines	?	0	Improper maintenance.
1996	747-100	Boeing	Trans World Airlines	16,869	230	Explosion of a fuel tank due to an electrical spark in a fuel tank.
2002	747-200	Boeing	China Airlines (Taiwan)	21,400	225	Improper repair of fuselage skin.
2008	747-400	Boeing	Qantas Airways	?	0	Burst oxygen tank.
2009	737-300	Boeing	Southwest Airlines	42,500	0	Fatigue cracking at a chemically milled step.
2011	737-300	Boeing	Southwest Airlines	39,786	0	Poor manufacturing; a sixty-inch unsupported gap of the crown splice skin; and the inspection policy in effect.

While fatigue specialists are used to consider structural integrity aspects of the aircraft that can cause the sudden decompression, the sudden decompression could cause passengers and flight crew to lose consciousness, due to a lack of oxygen at high altitudes. The FAA issued advisory circular AC 61-107A in 2003 to address the topic, which was later modified in 2013 to AC 61-107B. In 2015, the FAA issued AC-61-107B CHG 1, which is currently in use.In the full length paper [25] the author highlights sudden decompression as additional threat to the safe operation of an aircraft, with special focus on fuselage skin longitudinal lap joints design.

2.4 Influence of Finite Width Dimensions on Mutual Interaction of Two Opposing Cracks at a Hole (C. Matias and D. Elmalich, IAI)

Holes in structure are prone to fatigue cracking. Usually cracks will develop at both opposing sides of a hole, such that for some period, the two opposing cracks might grow simultaneously and influence each other, i.e. have mutual interaction. Accounting for this interaction might have significant impact on analytical results of cracking growth life, compare to not accounting for it.

This study evaluates the influence of the Finite Width edge effect on this mutual interaction. The study presents dual effects of the Finite-Width edge upon that interaction. One effect is that the edge causes enhancements to Stress Intensity Correction Factor (β) for the crack growing towards it, and thus also the accompanying opposing crack will be influenced by it. The other effect is that an edge creates an influence upon that interaction of not to be fully developed, as it would have been for an infinite width configuration. For infinite width dimensions, cracking growth life may factor up to 2, for not accounting of this two opposing cracks mutual interaction compare to accounting of it (see Figure 4).

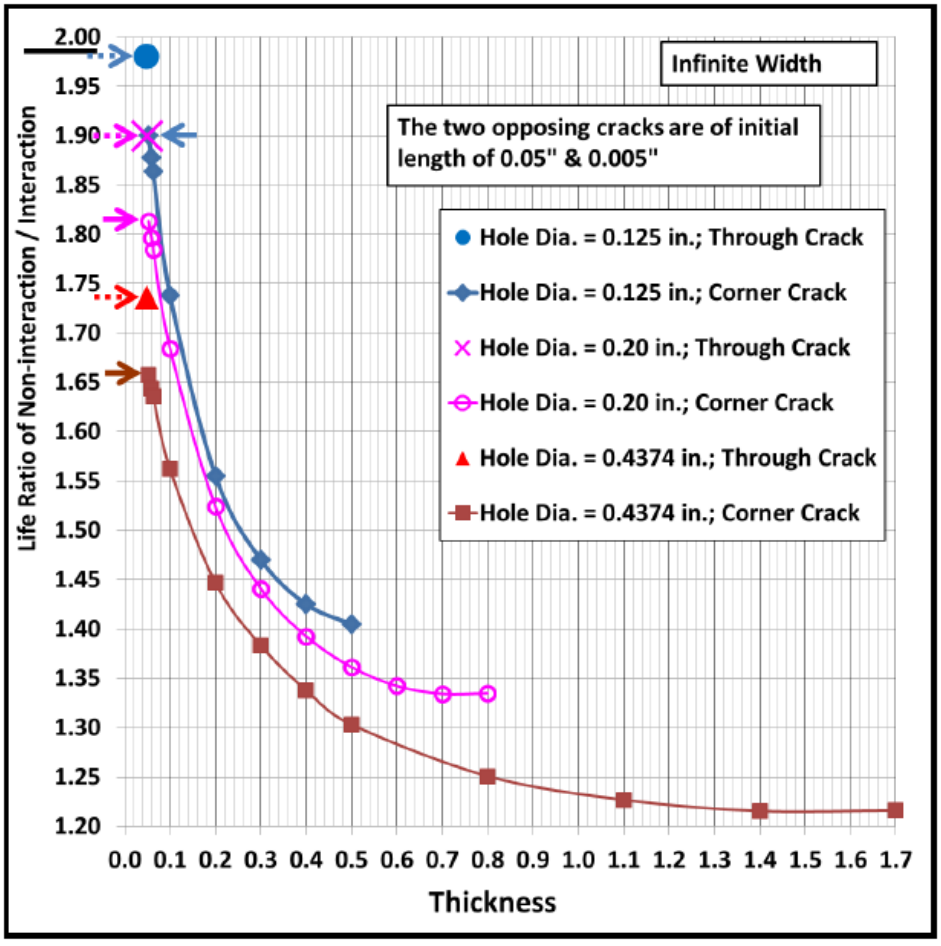

Figure 4. Two Opposing Cracks at a Hole, Life Ratio ([Non-interaction Analysis] / [Interaction Analysis]), per Plate Thickness (for CC) and Hole Diameter, for Infinite dimensions

For Finite Width dimensions (having the hole close to an edge), these dual effects are causing this cracking growth life factor to be reduced, but, to be increased again if the hole is "too close" to the edge.

For structural configurations having a hole near an edge of typical recommended adequate edge distance (of double the hole diameter), this factor is evaluated to be dropped up to 1.3. But, for shorter hole-to-edge distance this life factor will increase again. For hole-to-edge distance of 1.25 times the hole diameter, this life factor will increase back up to 1.8.

More conclusions of this study are drawn in the full length paper [26].

2.5 Examination of Algorithms for Prediction of Very High Cycle Fatigue Life (Y. Buimovich, IAI)

With the progress in technological development, a great number of machinery components, such as axle, wheel, gear, blade, etc., are expected to have a Very High Cycle Fatigue (VHCF) life beyond 10^7 cycles. Conventional fatigue testing to such high numbers of cycles would lead to excessively long test durations. Recent development of piezoelectric fatigue apparatuses has drastically reduced test times. These machines are capable of producing 10^{10} cycles in less than one week (at 20 kHz), while it would take more than three years for the same test duration using conventional equipment.

Claude Bathias reported in 1999 [31] that steels can fail at stresses below their endurance limit at very high numbers of cycles contrary to the popular industry belief. Since then many experimental results, observations and theories have been reported in the literature. However, these remain both academic in the sense that no practical method to include VHCF into engineering design has been proposed. Furthermore, since the cost of such tests is relatively very high, companies that perform these tests do not usually share information on their results.

Early experiments using the piezoelectric equipment show that most materials do not have a fatigue limit at 10^7 cycles, but instead their fatigue strength gradually decreases as fatigue life reaches 10^8 – 10^{10} load cycles [32]. In light of the present knowledge about VHCF of materials, the conventional S–N curve with the asymptotic fatigue limit could be modified into the curves illustrated in Figure 5 [32], which are often referred to as duplex or multi-stage S–N curves. The slight difference between the curves, Figure 5(a) and (b), reflects two viewpoints as to whether the fatigue limit in the VHCF range exists, Figure 5(a), or not, Figure 5(b). The distinction is made between surface and internal failures. Broad experimental evidence suggest that in the absence of the stress raises on the surface, with increasing number of cycles there is a gradual shift from fatigue failures initiating from the surface towards those starting at the internal material defects and leading to the development of the

so-called "fish-eye" (see Figure 6) on the fracture surfaces. This situation can occur at relatively low stresses, when cyclic slip at the surface does not give rise to sufficient surface roughening.

The fatigue crack growth proceeds as follows: first, the crack initiates from a material defect; second, it grows within the fish-eye, intermittently and accordingly at a very slow rate with the assistance of hydrogen trapped by the inclusion (hydrogen embrittlement); third, when the size of the inclusion plus the fish-eye reaches a critical value then crack growth starts outside the fisheye without the assistance of hydrogen; and fourth, the crack rapidly grows to failure [32, 34].

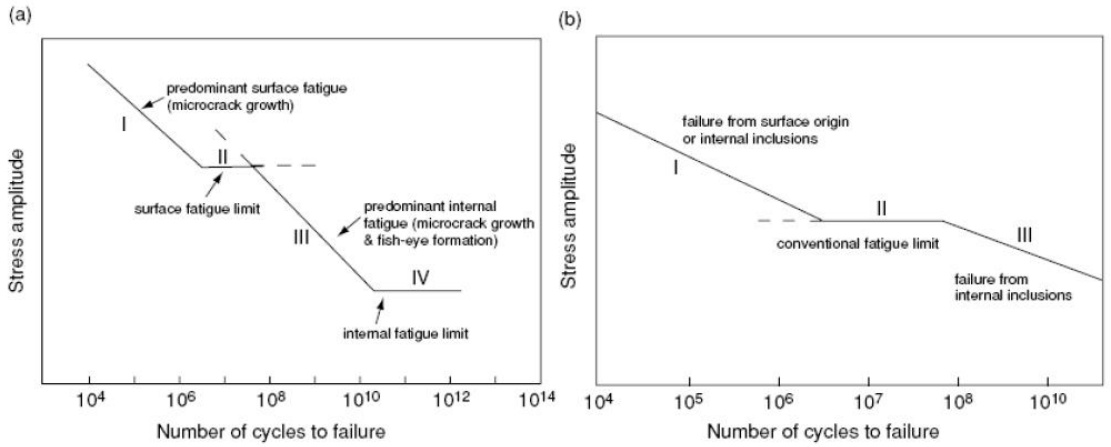

Figure 5. Schematic illustration of duplex S-N curve with (a) and without (b) fatigue limit in VHCF range. I-LCF; II-HCF; III and IV-VHCF (after [32])

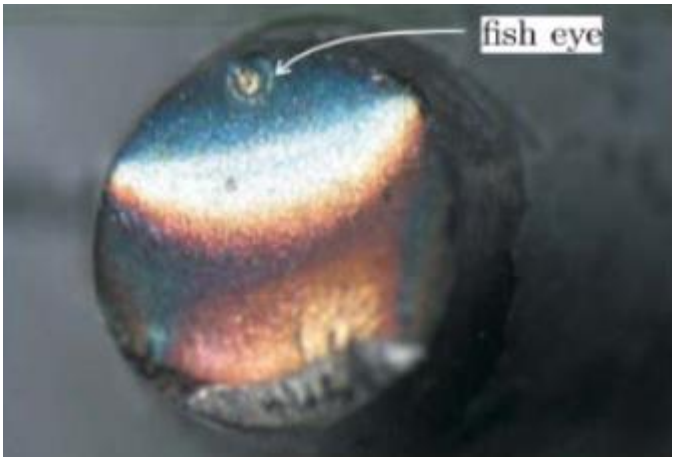

Figure 6. Fracture Surface in VHCF showing Fish-Eye [31]

This work is focused on the prediction of the S-N curve in VHCF, i.e. regions II, III and IV in Figure 5. Region I is the classic S-N curve in high cycle fatigue. Experimental data is widely available for many materials in HCF [35] and tests are relatively quick to carry out. Predictive methods are available, but because the mode of failure is different in HCF they are not applicable to VHCF.

For steels, one of the most supported views is the “hydrogen assisted crack growth” proposed by Murakami [34]. The method determines the maximum stress at which the stress intensity factor at the defect lies below the threshold value for crack initiation. It depends on only two basic quantities, namely the Vickers hardness Hv (kgf/mm^2) as the representative material parameter, and "$\sqrt{}$area" (μm) as the representative geometrical parameter for defects and cracks. The parameter "$\sqrt{}$area" is defined as the square root of the area obtained by projecting a small defect or crack onto a plane perpendicular to the maximum principal stress, and "$\sqrt{}$area$_{max}$" is the maximum possible value of "$\sqrt{}$area" for any inclusion in the material. Then, for R= -1, σ_w is given by

$$\sigma_w = 1.41\ (Hv + 120) / (\sqrt{}area_{max})^{1/6}$$

The S-N curve in VHCF lies between these two limit stresses, σ_{w0} and σ_w. To obtain the apparent high cycle fatigue endurance limit, σ_{w0}, shown as region II in Figure 5, there is a well-known estimation in terms of the Vickers Hardness, Hv, of the material. If the hardness is not known there is also a well-known estimation of this in terms of the ultimate tensile strength, UTS. These estimations are given in [34,36], for a stress ratio of R = -1 (fully reversed cycles), as

$$\sigma_{w0} = 1.6\ Hv \text{ and } Hv = UTS / 3.2.$$

There are conservative methods in the literature for calculation of VHCF life in metals [37,38]. In these methods, one should adjust the slope of the S-N curve calculated from classical S-N curves (for example [35]), after approximately 10^6 cycles according to a certain value, depending on the material. In [38], adjustment of the S-N slope after 10^6 cycles is determined as 1.25:10 log-log S-N curve and at 10^9 cycles, one should use 1 ksi for aluminum and 5% of Fty for steel.

An examination of the Murakami model for fatigue life calculation was carried out in this research and is presented in the full length paper [39]. This method will be compared to conservative methods for VHCF life calculations.

2.6 Why Should We Encourage Usage of Interference-Fit Fasteners at Airframe Structural Joints (C. Matias, IAI)

It is well established that using interference-fit fasteners will obtain longer fatigue lives to airframe structures, compare to using transition-fit fasteners (or close-tolerance) and certainly clearance-fit. However, common practical manufacturing considerations drive to less usage of the interference-fit fasteners. This is mainly due to the fact that manufacturing will encounter great deal of difficulties for the interference-fit fasteners installation (corresponding holes alignment, etc.). These difficulties are amplified for principal structural joints containing three member layers, as is for double shear splice joints (attachments of two separate spar sections or double shear skin splices, etc.). This means that where we mostly might need interference-fit fasteners, usually we will not use them. For such joints to have interference-fit fasteners, they will be installed using pneumatic steel hammering, in somewhat "aggressive" practical manner.

Process Specification (PS) for installation of interference-fit fasteners calls for fastener installation either by tapping the head with a plastic mallet or by driving the pin with a light rivet gun. Concerns were raised that practical "aggressive" installation procedures, might damage the holes such that the fatigue advantage will be insignificant, or even present fatigue disadvantages. There is lack of information for the influence on fatigue lives of the different practical installation methods for these interference-fit fasteners. Due to this concern, lack of relevant information and manufacturing requirements, there is tendency to design such joints not to use interference-fit fasteners, thus not to benefit of their fatigue advantages.

This study presents experimental investigation of test results supported by analyses, for the influence on fatigue life, of the following two parameters:

(1) The fastener-to-hole fit level, per % of diametric interference (positive diametric interference will mean that the fastener diameter is larger than the hole diameter, and the negative diametric interference will mean that the fastener diameter is less than the hole diameter, i.e. clearance).

(2) Two different fastener installation methods. The two fastener installation methods are: *hand plastic hammering* and *pneumatic steel hammering* as is practically used at the manufacturing line.

The study presents that the known fatigue advantage of obtaining longer fatigue lives for usage of interference-fit fasteners is being kept by the common manufacturing practice of fastener installation via the pneumatic steel hammering. Significant improvement in the fatigue life is presented for interference-fit fasteners installed via the pneumatic steel hammering compare to transition-fit fasteners installed via plastic hand hammering (and the reference open-hole specimens).

The study suggests positive relation between interference level to fatigue life, i.e., higher interference (per specification) contribute to longer fatigue lives, even for using “aggressive” pneumatic steel hammering. The very high analytical fatigue life results for interference-fit configuration (relative to open-hole configuration), suggests that any practical installation method (hand plastic or pneumatic steel hammering) is not a factor that is having significant influence on the fatigue life.

The study also suggests that any damage that might be induced to the hole by an "aggressive" installation procedure (as flaws in the hole bore) will have negligible growth (under typical aircraft loading spectra).

The conclusion from that study is that we should encourage usage of interference-fit fasteners, at structural joints, whenever fatigue life improvements are needed.

The full length paper, included in the proceedings of the ICAF 2019 symposium [40], will include full description of the test procedure, as well as the analytical/numerical derivations.

2.7 Analytical and Numerical Investigation of the Effect of Secondary Bending in Hard-Point Joints (Y. Freed, IAI)

Fuselage primary structural details are typically joined to each other by means of two major concepts. *Joints* (splices) are attachments in which the load is transferred from one member to another. Typical joints that may be found in fuselage structures are circumferential splice butt-joints and longitudinal skin lap-joints. *Hard-points* are attachments in which the load is jointly carried by two or more members. Typical hard-points that may be found in fuselage structures are skin-doublers attachments and skin-stringers attachments.

Due to cabin pressurization, membrane stresses are induced in the skin sheets every flight. Fastened attachments such as those described above include inherent eccentricity with respect to the load path, which induces **out of plane deflections** of the skin sheets. This is referred to as *secondary bending*, and it is considered as a side effect of tensile membrane loads acting on the skin. An example of typical secondary bending effect of a lap joint structure is shown in Figure 7. It may be noted that the secondary bending effect induces tensile stresses at the vicinity of the fasteners, which reduces significantly the crack initiation and crack growth lifetime of the joint.

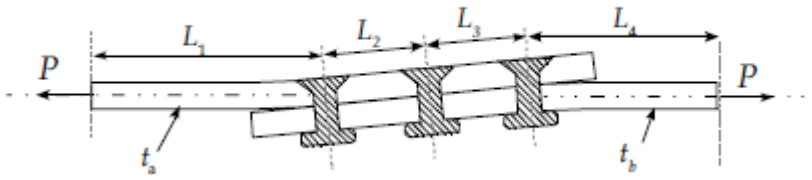

Figure 7. An example of secondary bending effect in a lap-joint attachment subjected to tensile loads.

The bending factor k is defined as the ratio between the bending stress and the tensile stress,

$$k = \sigma_{bending}/\sigma_{tenslie}$$

As discussed in [1], k can reach up to 3 for a case of a lap joint with a single row of rivets. This is a significantly increase of the stress level at the critical location of the joint. Indeed, the fatigue strength of riveted lap joints with two or more rivet rows, in which the bending effects are reduced, is significantly better than that with a single row of rivets. The secondary bending phenomenon is inherently different for lap-joints and hard-points attachments. Whereas the larger tensile loads are at the faying surface of a lap-joint connection, these are located at the inner skin surface for typical hard-point attachments, see Figure 8 for more details. From inspection point of view, it is understood that a lap-joint secondary bending scenario is considered as more critical than hard-point, due to the difficulty to inspect cracks at the faying surface.

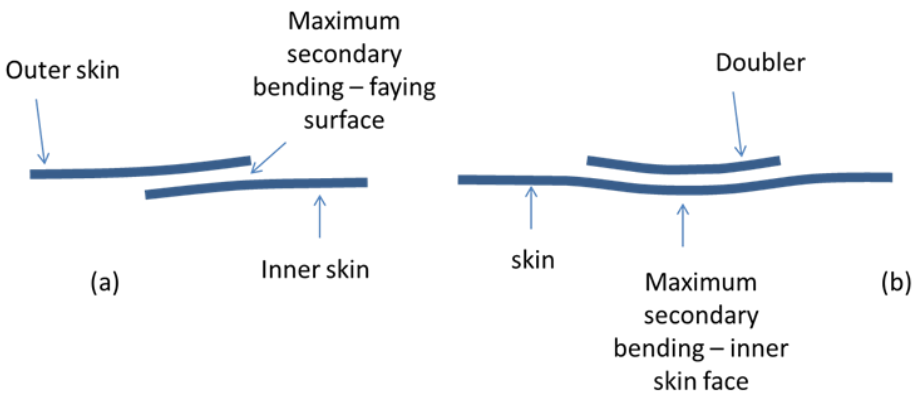

Figure 8. Illustrations of deformed shapes of (a) lap-joint and (b) hard-point attachments.

Although the effect of secondary bending was widely investigated for lap-joints attachment [42-48], both analytically/numerically and experimentally, the effect of this phenomenon on hard-point attachments is still not well established. In this study, the effect of the secondary bending on hard-point attachments is investigated analytically and numerically, and the parameter k is obtained for different geometrical combination and different hard-point scenarios (with and without skin cutout). Good agreement between analytical and numerical results is reported. The maximum ratio obtained numerically for typical fuselage configurations was derived as $\sigma_{bending}/\sigma_{tenslie} = 0.20$ (see Table 2 for more details), which is significantly lower than that obtained for lap joint attachments (that can reach up to $\sigma_{bending}/\sigma_{tenslie} = 3.0$). An example of an antenna installation is presented, showing significant decrease in the fatigue and crack growth lives due to the induced secondary bending effect.

Table 2. Numerical predictions of the ratio of $\sigma_{bending}/\sigma_{axial}$ $\sigma_{bending}/\sigma_{tenslie}$ for different panel and doubler thicknesses (in inches)

Sigma_B/Sigma_T

	Skin\Doubler	0.036	0.040	0.050	0.063	0.071	0.080	0.090	0.100	0.125
No Cutout	0.036	0.188	0.193							
	0.040		0.186	0.200						
	0.050			0.178	0.192					
	0.063				0.173	0.178				
	0.071					0.171	0.175			
	0.080						0.165	0.173		
	0.090							0.163	0.170	
	0.100								0.160	0.171
	0.125									0.156
	Skin\Doubler	0.036	0.040	0.050	0.063	0.071	0.080	0.090	0.100	0.125
With Cutout	0.036	0.142	0.146							
	0.040		0.141	0.145						
	0.050			0.134	0.141					
	0.063				0.131	0.134				
	0.071					0.130	0.132			
	0.080						0.128	0.131		
	0.090							0.126	0.129	
	0.100								0.125	0.130
	0.125									0.122

The numerical derivation of an hard-point secondary bending was presented in Ref. [49]. As part of the ICAF 2019 symposium, an analytical derivation of the secondary effect will be presented as well [50]. To this end, the neutral line model was employed, in conjunction with the effect of the fastener flexibility on the induced secondary bending (see Figure 9). Comparisons between analytical and numerical predictions are presented, and good agreement between the two approaches is achieved.

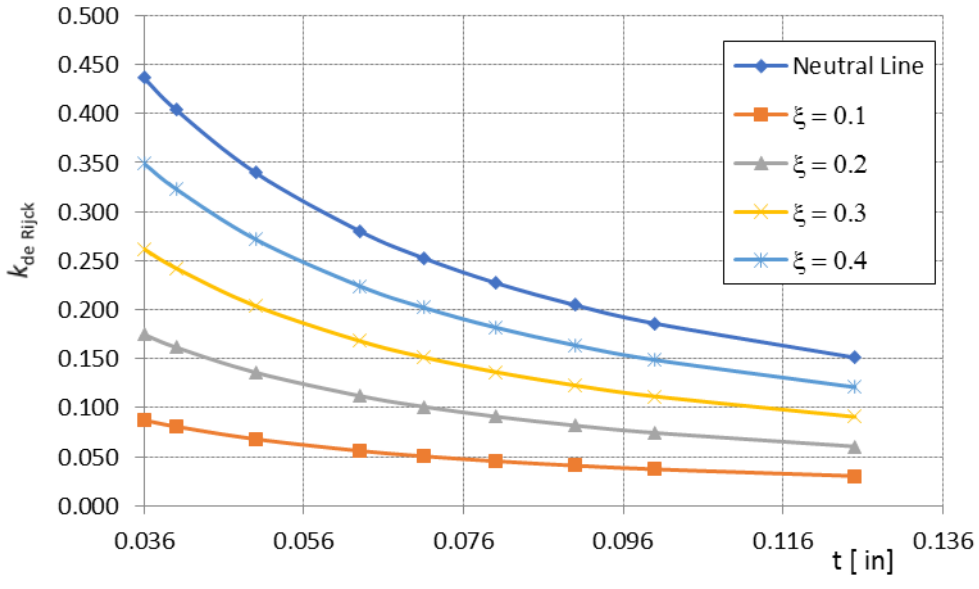

Figure 9. The ratio of $\sigma_{Bending}/\sigma_{Axial}$ for different fastener flexibilities

2.8 Research activities in Ben Gurion University – Mordechai Perl Group (M. Perl, BGU)

Prof. Mordechai Perl from Ben Gurion University (BGU) and his co-workers spend much research on different aspects of fracture mechanics related to pressure vessels in general, and to the process of autofrettage specifically. To this end, the distributions of the combined 3-D Stress Intensity Factor (SIF), $K_{IN}=K_{IP}+K_{IA}$, due to both internal pressure and autofrettage along the front of radial crack arrays emanating from the bore of an overstrained spherical pressure vessel were evaluated in Ref. [62]. The 3-D analysis was performed using the finite element (FE) method employing singular elements along the crack front. A novel realistic autofrettage residual stress field incorporating the Bauschinger effect was applied to the vessel. The residual stress field was simulated using an equivalent temperature field in the FE analysis. Similar investigation is presented in Ref. [66] with full or partial autofrettage on the combined 3-D SIFs for inner coplanar crack arrays and ring cracks in a spherical pressure vessels.

Three dimensional Mode I Stress Intensity Factor distributions along the front of a single inner radial semi elliptical crack emanating from the bore of an autofrettaged smooth gun barrel were evaluated in Refs. [63, 64]. The barrel was assumed to have been overstrained by either the Swage or the Hydraulic autofrettage processes. Here too, FE mode was employed as a simulation tool. Novel realistic overstrain residual stress fields, incorporating the Bauschinger effect, for the two autofrettage processes were applied to the barrel. The effect of material yield point and other plastic properties were demonstrated in Refs. [65, 67].

3. STRUCTURAL INTEGRITY OF COMPOSITE MATERIALS

3.1 Implementation of a Micromechanical Approach for Failure Predictions of Composite Materials (Y. Freed, IAI)

Composite materials are widely used in aerospace structures in recent years. These materials are characterized by high stiffness to weight ratio, can be tailored to a specific load conditions, and are relatively easy to shape for complex contours. Their major drawback, the relatively high cost as compared to metals, becomes less significant in recent years with the insertion of automation to serial production. Major development projects in recent years, such as Lockheed Martin F-35, Airbus A350 and the Boeing 787 models have an appreciable share of their structural components made of composite materials.

The current approach in substantiating aerospace structure made of composite materials is based on performance of a wide range of tests to establish material allowables in light of certain reliability and confidence levels. These are used as strength properties in the design phase. Later on during the development program, large scale tests (element scale up to full scale) are conducted to validate the design and as a 'proof of structure'. This methodology is commonly known as the 'building block approach'.

It is readily agreed that the building bock approach is time consuming, especially if the basis of the pyramid (material property development) is not in hand at the beginning of the development project. Analytical methods for prediction of material strength can replace part of the required testing, it these are shown to be reliable and accurate. All relevant aspects, such fabrication process, types of fibers and resins, volume fraction, operating environmental conditions and other aspects are discussed in [2]. In that study, also reported in the 2017 National Review [1], the 'trace method' and the 'Omni Strain Failure Envelope' were employed for the predictions of composite material stiffness and strength properties, and their accuracy was assessed and discussed. In the current study, the Strain Invariant Failure Theory (SIFT,[3,4]) is employed as a failure criterion for predictions of failures in composite materials. In the scheme of SIFT, critical failure properties of the different constituents of the composite material are first determined based on a small number of coupon tests. These are employed to predict the onset of damage initiation, progression and ultimate failure of a wide range of structural composite details which are subjected to complex loading conditions. The correlation between the micro-scale failure parameters and the macro-scale loading schemes is made by means of amplification matrices. These are obtained by means of FEM-based micromechanical approach. In the current study, the SIFT was generalized to incorporate the High Fidelity Generalized Method of Cells (HFGMC,[5]) as the micromechanical analysis procedure to determine the amplification matrices. The combined approach is called here as the 'HFGMC-SIFT' approach, that is schematically shown in Figure 10. The HFGMC-SIFT can be considered as superior to the standard SIFT due to the improvement in the micro-scale representation of the strain and the stress fields. The repeating unit cell is finer (64 cells as compared to 37), and the micromechanical approach is mostly analytically, as opposed to FEM-based approach in SIFT. In addition, the HFGMC-SIFT can account for the effect of thermal loading.

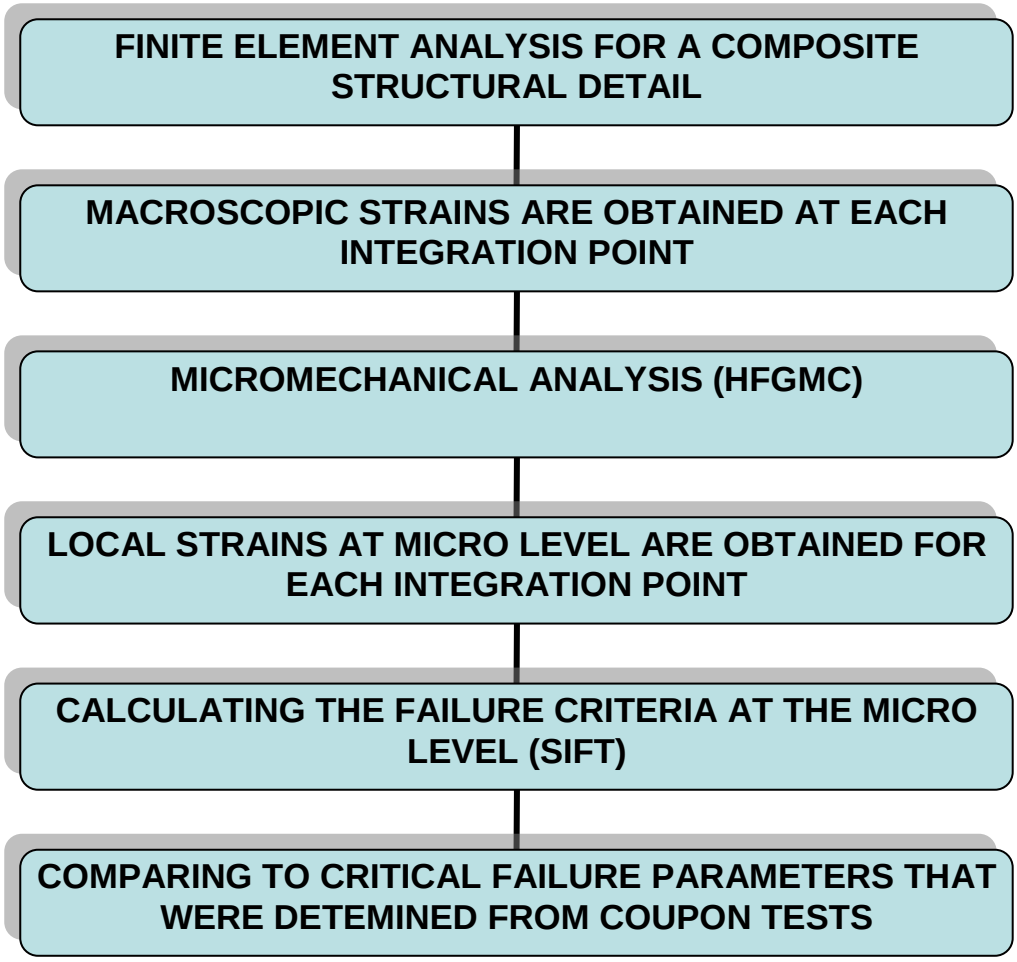

Figure 10. The HFGMC-SIFT approach

The HFGMC-SIFT performance was examined and compared to other failure predictions methods, such as SIFT-StressCheck [6], Super Mic-Mac and Tsai-Wu criteria[7]. The SIFT-StressCheck method was used by the US Navy for predictions of failures in composite materials, as reported in [6]. The Super Mic-Mac commercial software is used by Boeing to analyze failures in composite materials. Both methods are based on the SIFT micro-scale failure criterion. Their micromechanical procedure is based on a huge database of different materials and volume fractions. Finally, the Tsai-Wu criterion is a well-known macroscopic methodology to determine failures in laminated composites. It predicts at the macro scale, rather than the micro scale as the other approaches.

All predictions are summarized in Figure 11, in which P is the load for failure that was obtained by means of the failure analysis (HFGMC-SIFT, Super Mic-Mac, HFGMC-StressCheck or Tsai-Wu) and P_t is the force for failure as was measured in tests. It may be observed that the HFGMC-SIFT provides excellent accuracy, both with respect to experimental data and as compared to other approaches.

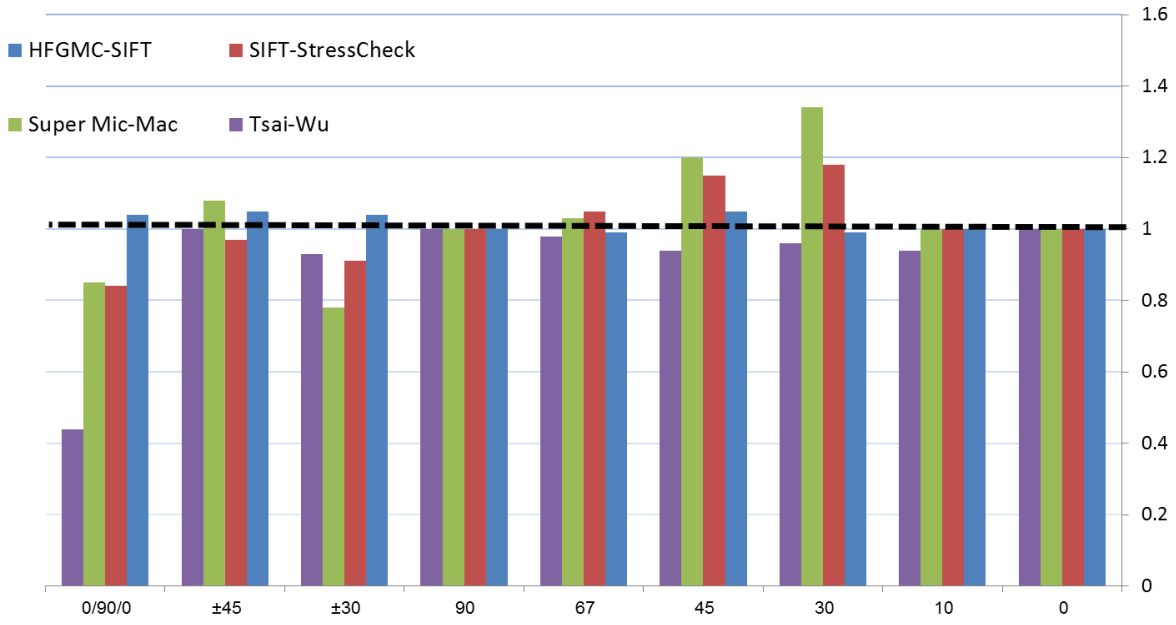

Figure 11. Failure predictions of several methods in terms of P/P_t.

The results presented in this study have shown that the proposed HFGMC-SIFT method is an accurate tool for predictions of failures in unidirectional composite materials. This approach requires relatively small amount of tests for calibration, and can be generalized for determination of strength properties every material stack-up. This eventually reduces the amount of testing required. However, it appears that the SIFT philosophy is suitable for structural elements which are subjected mostly to tensile loads. The failure mechanisms associated with compressive loads (such as micro-buckling) are not accounted for in the theory. Once the SIFT method is generalized to account more failure mechanisms it can be employed more intensively for determination of strength properties of composite materials.

This study was presented in the 58th Israel Annual Conference on Aerospace Sciences [8].

3.2 Examination of the KAWAI CLD Method for Fatigue Life prediction of Composite Materials (Y. Buimovich, D. Elmalich, IAI)

It is well known that aircraft structures are subjected to complex fatigue loading that accompanies changes in the amplitude, mean, frequency and waveform of stress cycling during service. Apparently, a large number of fatigue experiments under different kinds of cyclic loading conditions is required to elucidate the effect of loading mode on the composites sensitivity to fatigue; thus, this consumes considerable time and cost. Therefore, a time and cost-saving procedure for identifying the loading mode dependence of composites fatigue strengths is required. This procedure should assure reasonable accuracy on the basis of a minimal amount of test data.

It has been shown that the use of the linear Goodman curve for composites does not reflect the actual behavior of the material [9-13]. Hence, several methods were suggested for fatigue life prediction of composite materials over the past years [9-13]. Philippidis and

Vassilopoulos [11] presented a piecewise linear CFL diagrams for GFRP laminates. In this work, several R- ratios are considered. At each R-ratio the CFL values are determined from the S-N curve. The number of cycles at every two consecutive values or R ratio is connected with straight lines. Harris and his co-workers [10] developed semi-empirical equation based on fatigue test data for carbon fibers reinforced plastics (CFRP) and glass fibers reinforced plastics (GFRP) laminates. The equation includes several parameters that have to be calibrated based on empirical results of at least three R ratios. Boerstra [9] proposed alternative formulation that uses random fatigue data in which the R ratio is not a parameter in the model. The model includes five parameters that must be defined from a multi-objective optimization. Boerstra [9] did not specify the extent of the experimental data that is required or the effect of the data base on the prediction of the CFL diagrams. The studies mentioned above [9-11] have one major disadvantage due to the relatively vast data that is required, which consumes a great amount of tests. Kawai et al. [12,13] proposed a nonlinear CFL diagrams for several laminations that are based on one critical R-ratio and demonstrated this model on several layouts of carbon/epoxy laminates. In this method, fatigue tests are carried out at one critical R-ratio, defined as the ratio of the Ultimate Compression Strength (UCS) over Ultimate Tensile Strength (UTS) of the material. This critical ratio is called χ. This method is a time and cost-saving procedure that provides reliable data.

The Kawai formulation depends on the position of the mean stress, σ_m, in the domain $[\sigma_C, \sigma_T]$ as follows

$$-\frac{\sigma_a-\sigma_a^{\chi}}{\sigma_a^{\chi}}=\begin{cases}\left(\dfrac{\sigma_m-\sigma_m^{\chi}}{UTS-\sigma_m^{\chi}}\right)^{2-\psi_\chi} & UTS\geq\sigma_m\geq\sigma_m^{\chi}\\ \left(\dfrac{\sigma_m-\sigma_m^{\chi}}{UCS-\sigma_m^{\chi}}\right)^{2-\psi_\chi} & UCS\leq\sigma_m\leq\sigma_m^{\chi}\end{cases}$$

where, σ_a^{χ} and σ_m^{χ} are the alternating and mean stress components of the fatigue stress for a given constant value of life, N, under fatigue loading at the critical stress ratio, χ =UCS /UTS. The variable ψ_χ denotes the fatigue strength ratio and it is defined as

$$\psi_\chi=\frac{\sigma_{max}^{\chi}}{\sigma_b}$$

where, σ_b (>0) is the reference strength to define the peak of the static failure envelope in the (σ_m- σ_a) plane and σ_{max}^{χ} is the maximum stress extracted from the S-N curve of the critical R-ratio, χ, for a given number of fatigue cycles. The critical fatigue strength ratio represents the normalized cyclic stress, and its relation to the number of loading cycles defines the normalized critical S–N curve:

$$2N_f=\frac{2}{K^*}\frac{(1-\psi_\chi)^a}{\psi_\chi^{\,n}}$$

where the constants a, n and K* are material constants determined iteratively.

Static and fatigue tests were carried out for open-hole coupon specimens made of unidirectional carbon/epoxy tapes for examination of the applicability of the Kawai constant life model. A quasi-isotopic lay-up of intermediate modulus unidirectional (UD)

Carbon/epoxy tapes was examined. The lamination sequence, [(+45°, 90°,-45°, 0°)s]s, is balanced and symmetrically stacked. The geometry of the specimens was in accordance to ASTM standard for open-hole tests (ASTM D5766, ASTM D6484). A total of 56 composite specimens were tested. The tests included static compression and tension strength to obtain the critical R ratio. Fatigue tests included five R ratios; i.e., 0.5, 0.1, χ, -1 and -10. Most R-levels consisted of five levels of stresses (with two tests at each stress level). A picture of the tested specimen at the loading apparatus is given in
Figure **12**.

Figure 12. The tested specimen at the loading fixture

The predicted Kawai CFL and test results of fatigue tests are shown in Figure 13. Note that the values of the mean and amplitude stress in Figure 13 are normalized with respect to the reference stress σ_b. A relatively good agreement was obtained between the predicted and experimental results, with the exception of R=-10. The prediction of the Kawai model was slightly conservative for R-ratios $\geq$-1 and un-conservative for R-ratio that equals 10.

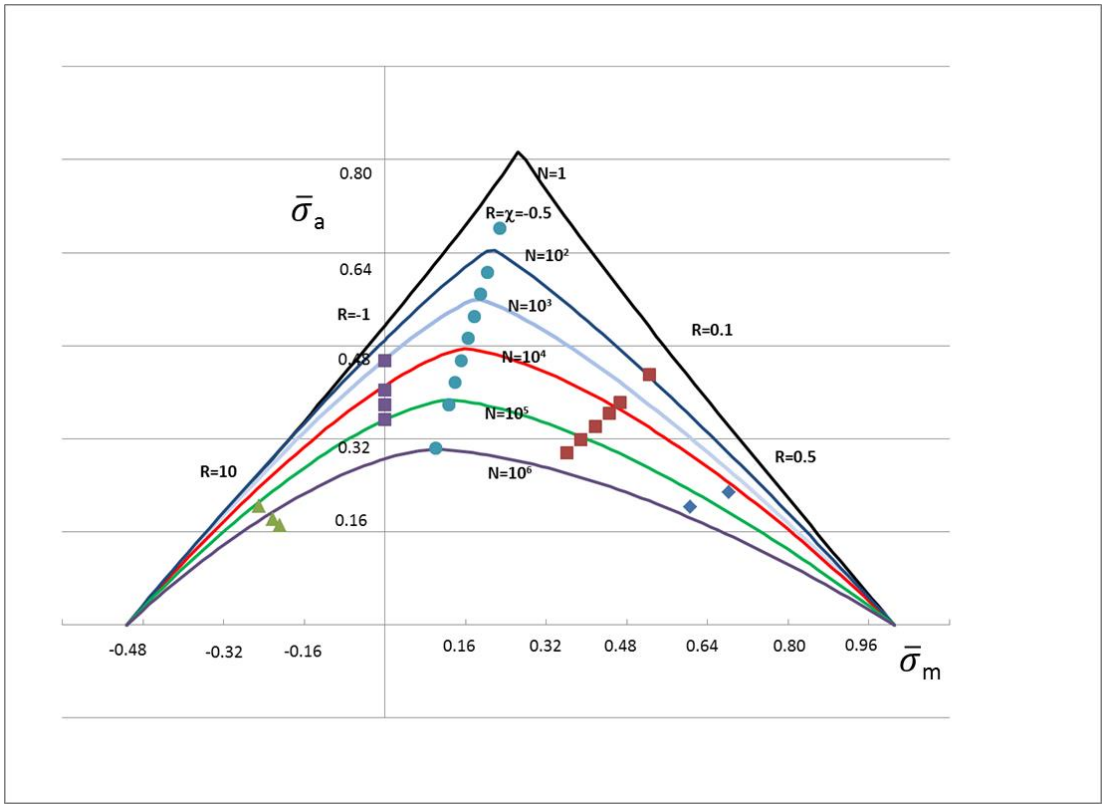

Figure 13. Kawai Constant Fatigue Life Diagram for unidirectional Carbon/epoxy laminates

As part of this study, a modified model was proposed to overcome the un-conservatism of the Kawai model at the pure compression zone. Thus, the constant life curve is built from two parts; i.e. for UTS $\geq\sigma_m \geq \sigma_m^{\chi,}$ constant life diagrams are built according to KAWAI method and for UCS $\leq\sigma_m \leq \sigma_m^{\chi,}$ constant life diagrams are built by a linear line between σ_a^{χ} and UCS. Hence, CFL formulation is determined as follows

$$-\frac{\sigma_a-\sigma_a{}^{\chi}}{\sigma_a{}^{\chi}}=\left(\frac{\sigma_m-\sigma_m{}^{\chi}}{UTS-\sigma_m{}^{\chi}}\right)^{2-\psi_{\chi}} \qquad UTS\geq\sigma_m\geq\sigma_m{}^{\chi}$$

$$\sigma_a=(\sigma_m-\sigma_c)\times\frac{\sigma_a{}^{\chi}}{\sigma_m{}^{\chi}-\sigma_c} \qquad UCS\leq\sigma_m\leq\sigma_m{}^{\chi}$$

.

The predicted modified Kawai CFL and test results of fatigue tests are shown in Figure 13. Figure 14 clearly reveals that the experimental results of R=10 are within the range of the CLD, as opposed to these values in Figure 13.

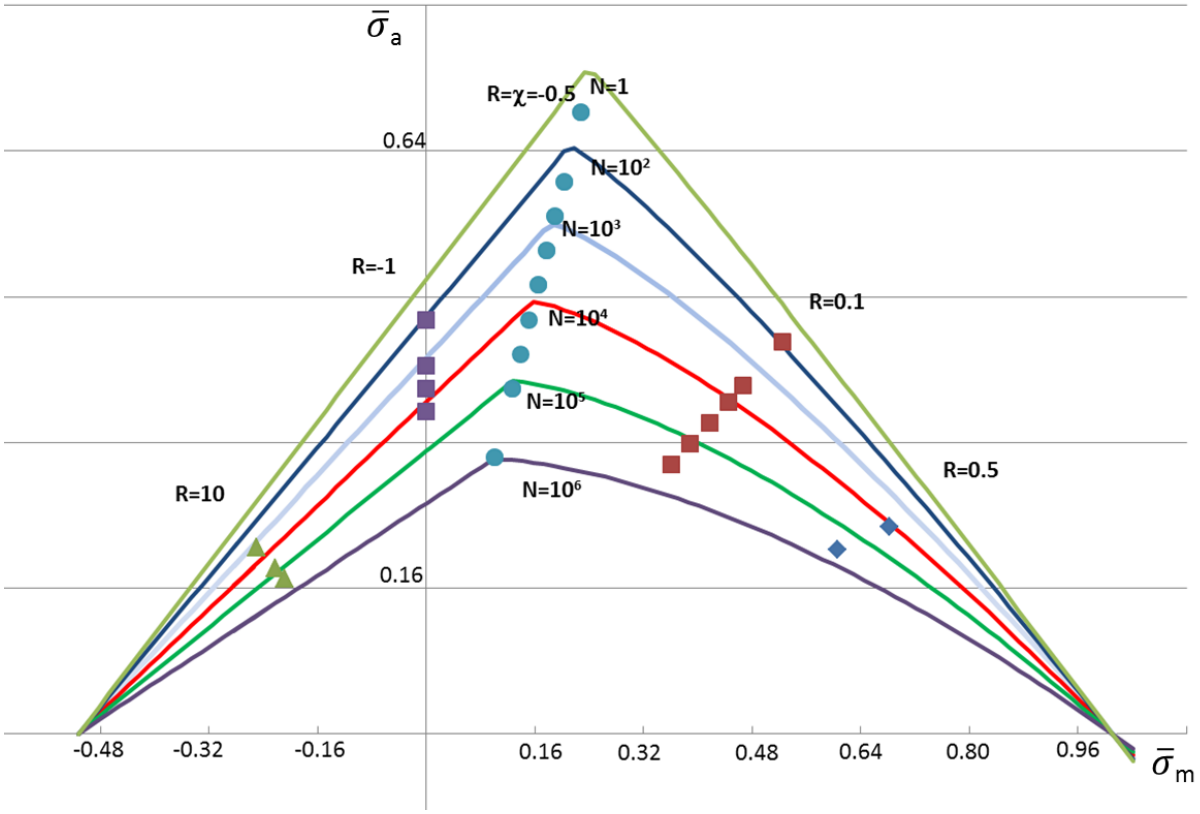

Figure 14. Modified Kawai Constant Fatigue Life Diagram for unidirectional Carbon/epoxy laminates

To conclude, the applicability of Kawai CLD method for fatigue life prediction of composites was examined. Fatigue tests were conducted at the critical R-ratio for modeling the constant life diagrams, per Kawai method, as well as at different R-ratios, used for validation. The predictions of the Kawai model were slightly conservative for R-ratios ≥-1 and un-conservative for R-ratio that equals 10. A modified model was suggested to overcome the un-conservatism of the Kawai model at the pure compression zone. The predicted curve of the modified model was compared to the experimental results and was shown as conservative for fatigue life greater than 10^5. Hence, with application of the appropriate scatter factor, the use of the modified Kawai model is considered relatively accurate.

This study was first reported in the 2017 National Review [1], and was presented in the 58th Israel Annual Conference on Aerospace Sciences [14]. Several updates and new developments will be reported as part of the ICAF 2019 symposium [29].

3.3 A Multiscale Progressive Damage Analysis for Laminated Composite Structures Using the Parametric HFGMC Micromechanics (J. Aboudi, R. Haj-Ali, TAU)

Predicting the mechanical response and failure behavior of fiber-reinforced composite laminates is viable for efficient design in structural applications. By utilizing micromechanical approaches it is possible to capture the nonlinear mechanical response and progressive damage of composite laminates. The micromechanical analyses enable to account explicitly the effects of the composite microstructure, fiber volume fraction, packing, and

orientation. These approaches are robustic tools for the prediction of failure in composite materials and structures.

The parametric high fidelity generalized method of cells (HFGMC) micromechanical analysis is a generalization of the regular HFGMC that has been discussed and applied by Prof. Jacob Aboudi and his co-workers during the past two decades. This parametric HFGMC analysis, which has been recently developed by Prof. Haj-Ali and Aboudi from Tel Aviv University, involves local quadratic displacement fields within a discretized representative volume element (RVE) or unit-cell (RUC). This RUC is divided into a general assembly of hexahedral sub-volumes or subcells which can capture the local effects which results from the field gradients and the microstructure of the multiphase composite. In the framework of the HFGMC, equilibrium equations, interfacial and periodic displacements and tractions at the boundaries of the RUC are imposed in the average sense. The HFGMC approach is general enough and can be employed in conjunction with any nonlinear constitutive model for both deformation and damage.

Micro-buckling fiber-reinforced composite laminate results from axial compression. A number of analytical formulae have been proposed to predict the strength of unidirectional composites subjected to compression, see [16-20]. According to these studies the important parameters affecting the compressive strength of unidirectional composites are the fiber volume fraction, fiber diameter, fiber misalignment, fiber/matrix interface strength, and the matrix shear modulus. Existing and new micromechanical models have been integrated with the finite elements for multi-scale analysis. In this computational approach, the behavior of the composite at the micro-scale is integrated with macroscale structure analysis, such that the two coupled scales are simultaneously solved. Therefore, an explicit representation of the material is considered at the microscale level by employing micromechanics whereas at the macro-scale level the complex geometrical structure with various boundary conditions is modeled and solved by a standard displacement-based FE code. Obviously, the high computational cost is the significant drawback of this approach.

In the present investigation, a nonlinear multiscale analysis based on the parametric HFGMC micromechanical approach coupled with the FE code, is proposed for the prediction of the response and progressive damage in composite laminates. The compressive strength of unidirectional composites proposed by Lo and Chim [19] has been applied to determine micro-buckling compression failure of an individual lamina within the composite laminate. Furthermore, both the Tsai-Wu [15] and SIFT in conjunction with the cell extinction damage (CED) [2] approaches were applied, to determine the failure of an individual composite lamina due to fiber, matrix, or in-plane shear failure modes.

The responses and strengths of laminated composites to applied loadings are obtained by utilizing the above proposed multiscale analysis. In order to assess the efficiency of the proposed multiscale analysis, three different open-hole laminates subjected to compression and tension are investigated. To this end, three multidirectional manufactured from

carbon/epoxy (IM7/977-3) system and tested by the Air Force Research Laboratory (AFRL), were considered. In these laminates, the value of fiber volume fraction of 60% is used.

A comparison between the stress-strain responses obtained by the experimental investigation and the present multiscale approach, based on the calibrated material constants, for ±45º laminate, subjected to uniaxial tension, and 0º laminates subjected to both uniaxial compression and tension, are shown in Figure 15 and Figure 16. It should be noted that the longitudinal compression response of the IM7/977-3 lamina does not show a sufficient agreement with the
experimental study. Furthermore, the measured compressive strength of the lamina is lower than the predicted micro-buckling criterion. These disagreements may be attributed due to fiber misalignment, existing defects, or waviness within the lamina.

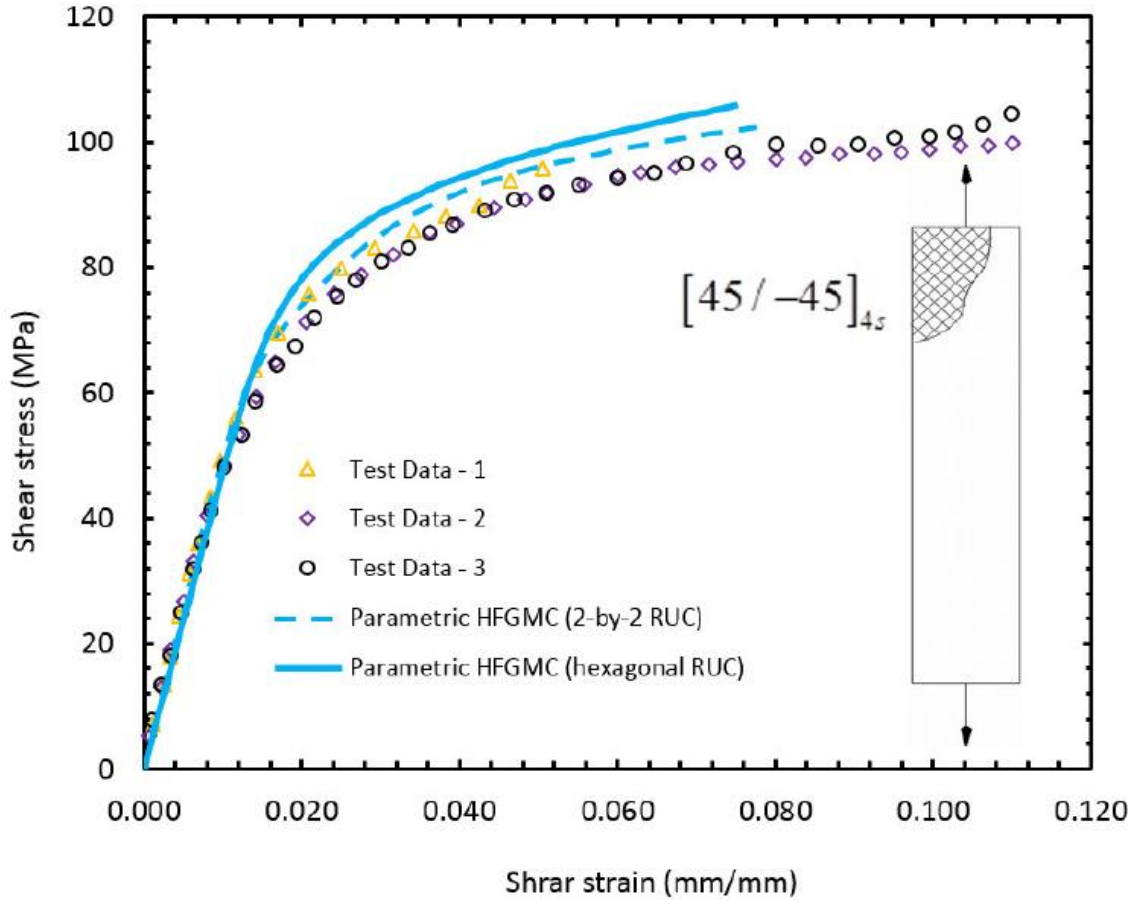

Figure 15. Composite shear stress-strain response from ±45º tension

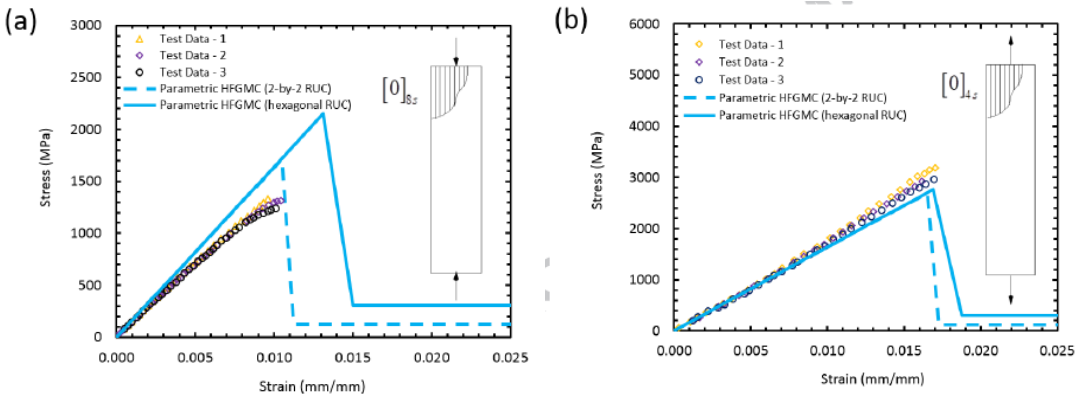

Figure 16. Composite normal stress-strain response from 0º (a) compression and (b) tension.

Figure 17 shows the damage evolution within the lamina, subjected to tension applied in the transverse direction to the fibers. This was compared to available data in the literature and good correlation was demonstrated.

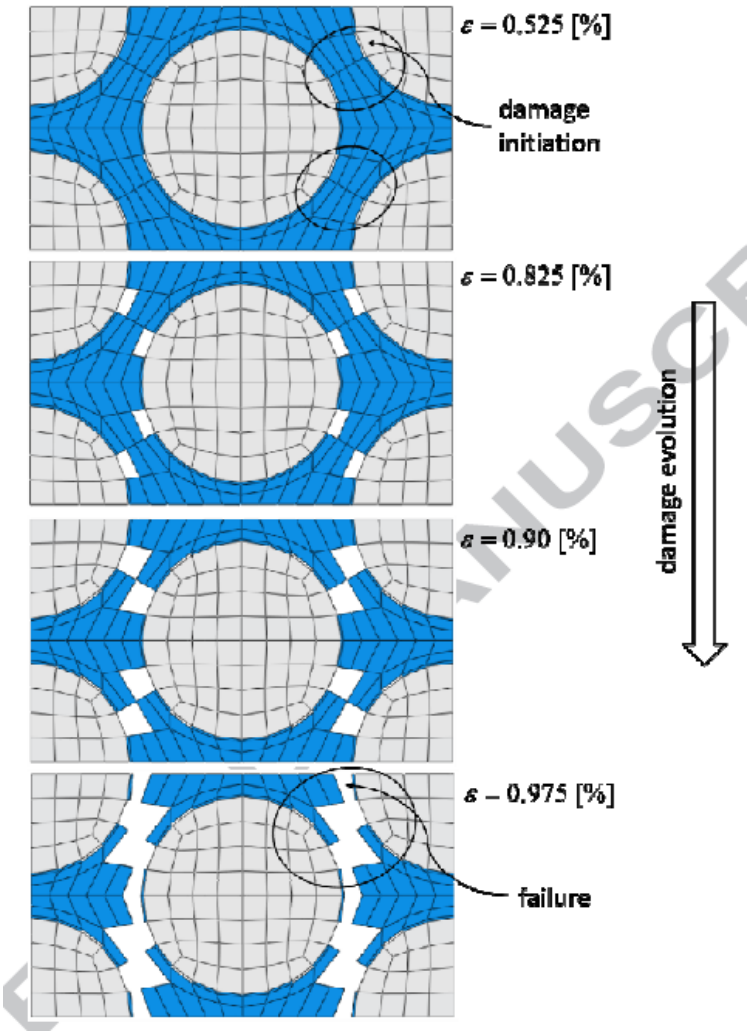

Figure 17. Damage evolution for composite normal stress-strain response from 90º tension (SIFT local failure criterion and CED).

The full length paper [21] was accepted for publication in Composite Structures.

3.4 Semi-analytical Compressive Strength Criteria for Unidirectional Composites (J. Aboudi, R. Haj-Ali, TAU)

The compressive strength of unidirectional composites is strongly influenced by the elastic and strength properties of the fiber and matrix phases, as well as by the local geometrical properties, such as fiber volume fraction, misalignment, and waviness. In the present investigation, two microbuckling criteria are proposed and examined against a large volume of measured data of unidirectional composites taken from the literature. The first criterion is based on the compressive strength formulation using the buckling of Timoshenko's beam. It contains a single parameter that can be determined according to the best fit to experimental data for various types of polymeric matrix composites. The second criterion is based on buckling-wave propagation analogy using the solution of an eigenvalue problem. Both criteria provide closed form expressions for the compressive strength of unidirectional composites.

The study proposes modifications of the two criteria by a fitting approach, for a wide range of fiber volume fractions, applied to four classes of unidirectional composite systems. Furthermore, a normalized form of the two models is presented after calibration in order to compare their prediction against experimental data for each of the material systems. The new modified criteria are shown to give a good match (within the practical volume fraction of 0.3 to 0.7) to a wide range of unidirectional composite systems, as shown Figure 18.

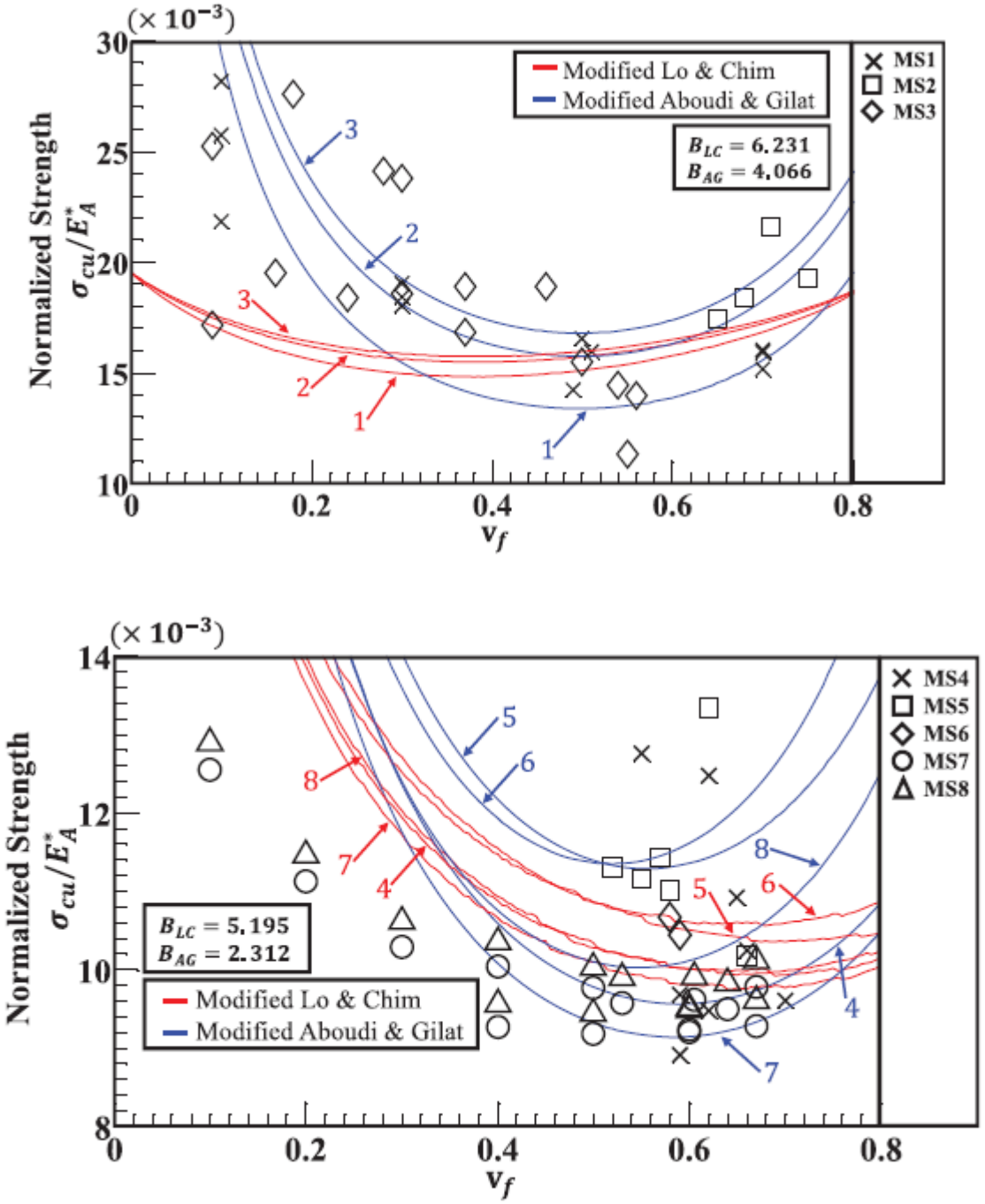

Figure 18. Normalized compressive strength versus fiber volume fraction for GFRP (top) and CFRP (bottom) composites

The full length paper [23] provides the entire analytical derivation as well as its validation and verification as compared to various test results.

4. PROBABILISTIC STUDIES

4.1 Nearly Identical Twins or Distant Cousins, Revisited. Weibull or Log-Normal Distributions to Characterize Fatigue Life Scatter – Which is Recommended? (A. Brot, Brot Engineering Consultant)

Brot presented the Plantema Memorial Lecture in ICAF 2017 symposium in Nagoya. Its lecture included, among others, a topic entitled "Nearly Identical Twins or Distant Cousins?" which dealt with the differences between the Weibull and Log-Normal distributions, both of which are meant to deal with fatigue test scatter.

The current paper describes further developments on this topic, including a tentative conclusion on which distribution is more correct. One of the downsides of using fatigue life methodology to determine the safe-life, is that considerable scatter exists, which needs to be accounted for in determining the life to crack initiation. SuperSMITH Software has been developed by Fulton Findings to analyze several statistical distributions, including obtaining their statistical parameters and plotting their results. This software is based on the theoretical methods described in the "New Weibull Handbook" [27].

By comparing the results shown in Figure 19 to those shown in Figure 20, vast differences in the calculated safe-life exist between the two distributions. Obviously, both cannot be correct! Due to these great differences, the author developed a method to help determine which distribution is more accurate. A large fatigue-life database was constructed using test results of many fatigue tests, all composed of various aluminum alloys. In total, the database consisted of 86 specimens.

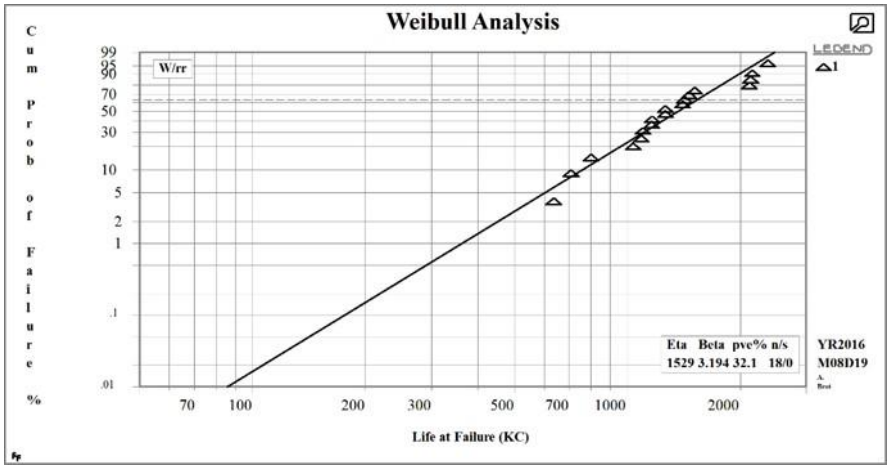

Figure 19. Weibull analysis performed by SuperSMITH Software1 indicates a Safe-Life of 86 KC (86,000 cycles) for a typical application.

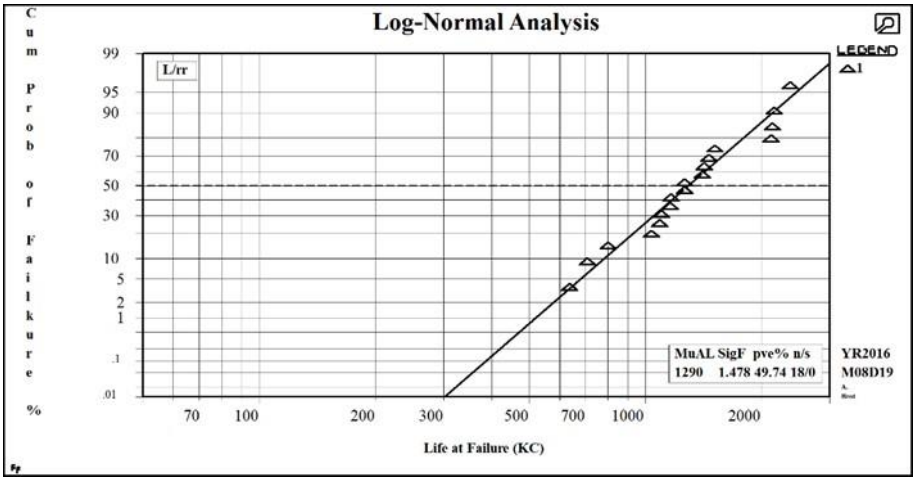

Figure 20. Log-Normal analysis performed by SuperSMITH Software1 indicates a Safe-Life of 300 KC (300,000 cycles) for the identical application.

The above mentioned 86 fatigue test results were combined to result in a single test result. The 86-fatigue test lives were normalized to result in a "Characteristic Life" of 50,000 cycles. The lowest failure among the 86 virtual specimens was at 18,975 cycles, while the highest failure was at 99,784 cycles. Weibull and Log-Normal plots (Figure 21 and Figure 22) were built for the 86-specimen database, again using SuperSMITH Software.

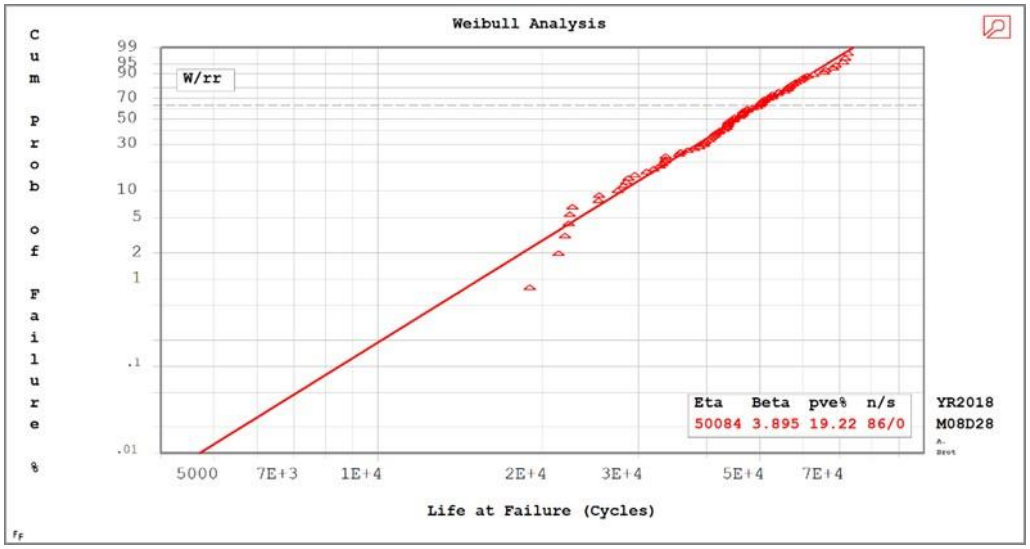

Figure 21. Weibull plot for the 86-specimen test, indicating a safe-life of about 4,700 cycles.

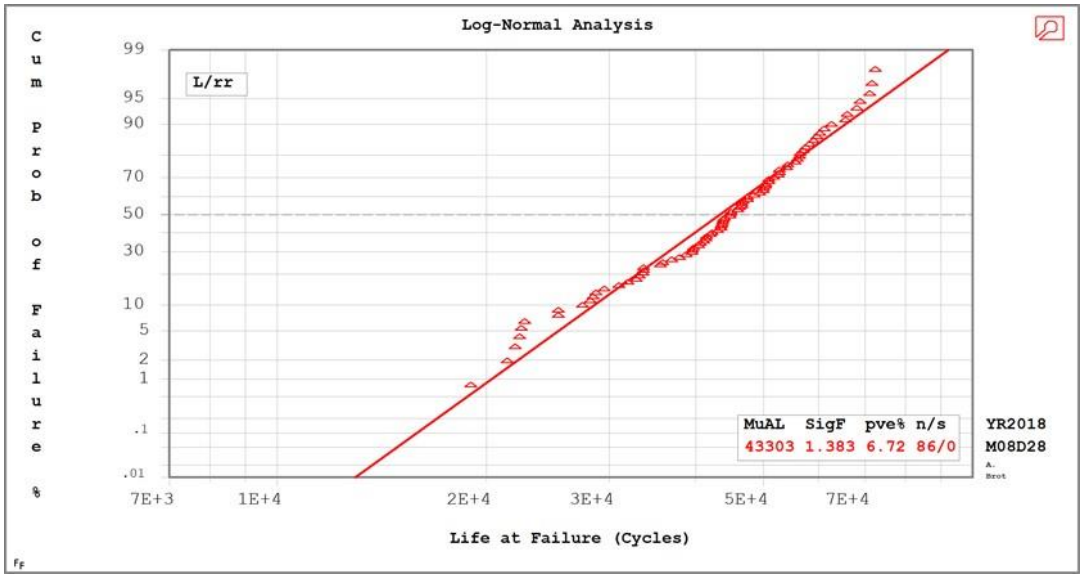

Figure 22. Log-Normal plot for the 86-specimen test, indicating a safe-life of about 13,000 cycles.

The two safe-life calculations differed by a factor of 2.7, which is unacceptable!

In order to analyze which is the more accurate distribution, the data of Figure 21 and Figure 22 were replotted on log-log axes, as is shown in Figure 23.This figure indicates that six of the eight earliest failures, which are below the 10% probability of failure line, clearly indicated that the **Weibull distribution is more accurate** than the Log-Normal distribution, when dealing with fatigue failures. In addition, two other considerations point to additional benefits of utilizing the Weibull distribution when dealing with fatigue-life failures to determine the safe-life:

- The Weibull distribution is always more conservative than the Log-Normal distribution.

- Comparing both distributions, per Figure 21 and Figure 22, shows that the "pve parameter" of the Weibull distribution is 19.22% while that for the Log-Normal distribution is only 6.72%. The "pve parameter" measures the goodness of fit between the failure points and the distribution values. The New Weibull Handbook (5th edition) [58] states that "*a pve value of less than 10% indicates a bad fit*". Since the Log-Normal distribution has a pve value of only 6.72%, this indicates that there is a very poor correlation for the Log-Normal model for this application.

In view of these results, the author concluded (tentatively) that the Weibull distribution should be preferred to determine the safe-life of a fatigue-critical structural member that has undergone fatigue testing. More details and explanations are provided in the full length paper, that was presented in [30] and will be further explained and presented in the ICAF 2019 symposium [28].

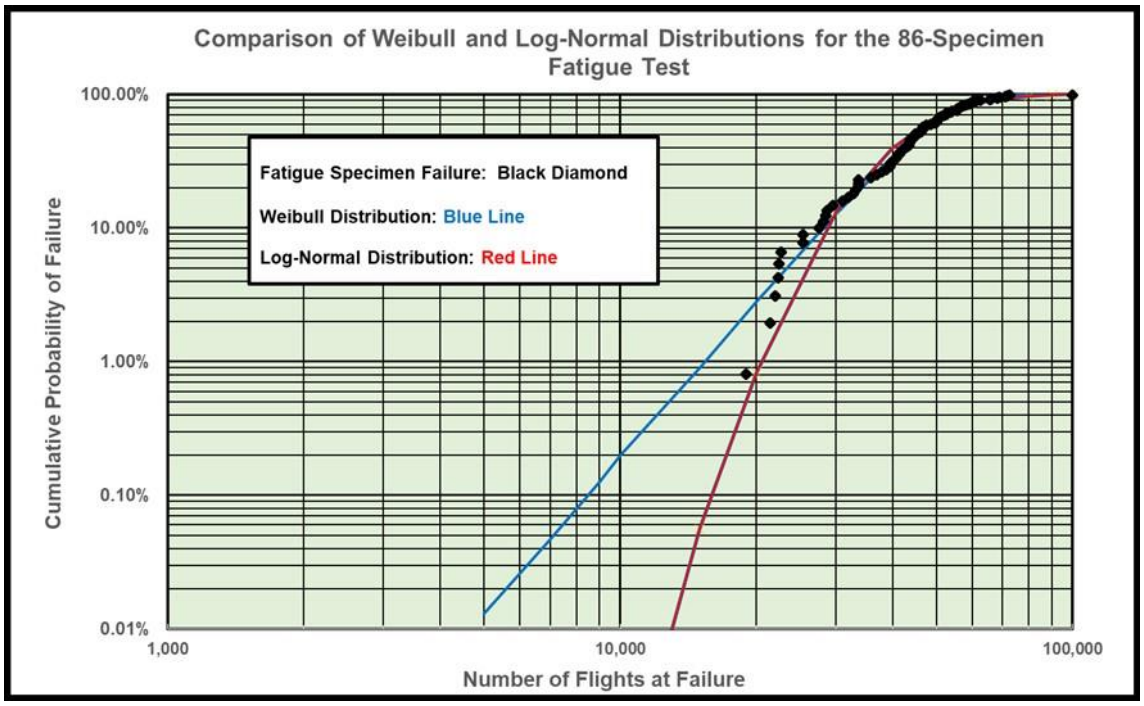

Figure 23. Weibull and Log-Normal plots for the 86-specimen test.

5. STRUCTURAL HEALTH MONITORING

5.1 Characteristics Pattern Recognition Algorithm for Health and Usage Monitoring (B. Dorfman, S. Shoham, I. Kressel, G. Don-Yehiya, IAI, M. Tur, TAU)

This study introduces multipurpose structural characteristics pattern recognition algorithm that can be used as load and usage monitoring tool, health monitoring tool and shape sensing. The algorithm is based on online measurements of strain using electrical strain gauges or more advanced fiber optic Bragg Grating (FBG) sensors. A statistical based mechanism is used to determine the state of the structure at any time during flight. Understanding of the physical condition being monitored is used to establish key parameters of the algorithm such as dictionary function time windowing and others. The algorithm utilizes pattern recognition by representing every instantaneous strain readings as a superposition of known structural characteristics such as typical aircraft maneuvers, normal modes, etc. Statistically based methods are used to reveal the damages, characterized by strain readings outside the statistical normal deviation. Statistical analysis is provided as a tool to establish alert indications without directly determines of limit values for each operation condition. Other properties of the flight such as load rates and displacement state at a given tine can be obtained based on this method as well.

The algorithm is based on an assumption that some characteristics of the sampled data are known. This concept is identical to the fundamental approach used in compressing sensing, where the measured signal is described by a superposition of known signals, called the dictionary. Such known characteristics can be, for example, the normal modes, known flight conditions etc. More details on the derivation of this algorithm are provided in Ref. 22. This algorithm was employed as part of IAI SHM program, in which the UAVs were equipped with fiber optic based FBG sensor net.

A finite element analysis was used to validate the presented concept. The simulation contained a detailed model of the boom while all other structural elements are modeled as "stick model" and FBGs are modeled as 1D elements. All FBGs used in the UAV SHM demonstrator are located in the model as well as additional FBGs to better optimize FBGs arrangement effects.

FBGs are located along the length of the boom at 15 stations (**Error! Reference source not found.**). On each station 4 FBGs are placed, top (1 through 15) bottom (16 through 30) inboard (31 through 45) and outboard (46 through 60). The simulations first run contains a modal strain analysis read at the FBGs elements. These are used as dictionary function. Later, several different dynamic analysis were performed to describe different proper landing stats. Finally several different types of damage were introduced to the model and the dynamic landings analysis was repeated. Shown later on are results obtained from one type of damage, the regarded damage is a lack of main load caring element on the FBGs longitudinal station.

It is assumed that the booms behavior during landing can be described by four modes: general bending, torsion, 1st bending mode and the 2nd bending mode. The proposed algorithm was employed based on the FBG measurements, where standard deviation of the differences vectors for "healthy" statistical range was found to be bounded by $3\sigma = 11.7\mu\varepsilon$. An illustration of "healthy" structure measurements is shown in Figure 24.

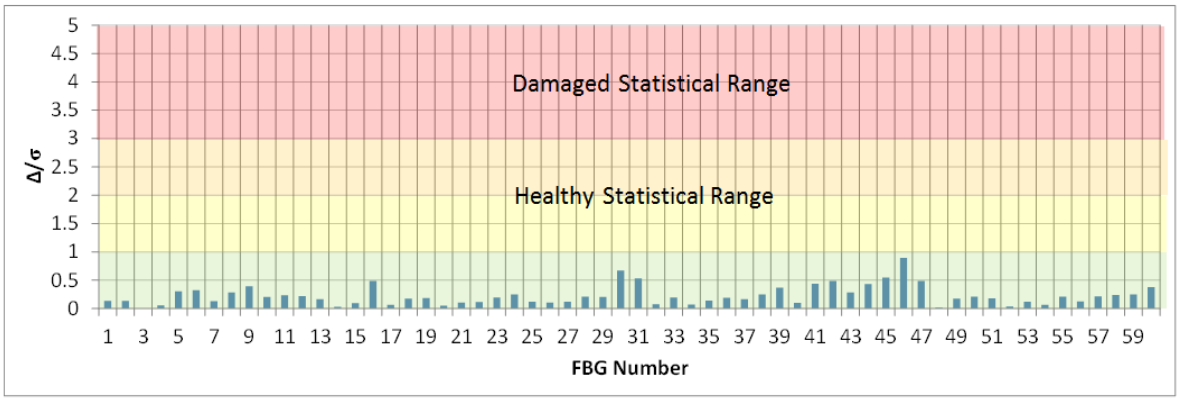

Figure 24. Δ_m/σ plot for "healthy" structure

It is evident that for "healthy structure all FBGs have averaged differences below σ. As a result, the observer can conclude that the structure is healthy. On the other hand, similar plot is provided for "damaged" structure in Figure 25. It is clear that FBG 34 is within the damaged statistical range. Despite FBG 4 has $\Delta_m < 3\sigma$, it can be also suspected as damaged. This is because it has deviation which is much higher than typical: all other FBGs are within healthy statistical range. One may pay attention that FBGs 4 and 34 are located at the same station in the vicinity of the damage, and therefore it is reasonable that both of these FBGs are suspected as "damaged".

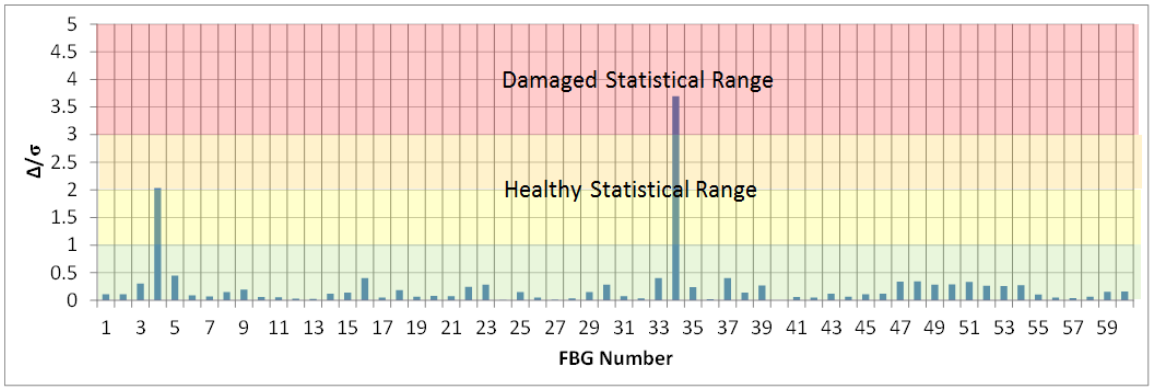

Figure 25. Δ_m/σ plot for "damaged" structure

To conclude, the algorithm was found to be a good SHM tool for identification of FBGs close to the damage. The algorithm, however, is only on its initial stage of development and promises great potential. Nevertheless, algorithm stages should be better studied and deeply to understand, for example, the sensitivity of the algorithm to appropriate choosing of dictionary vectors, and position of gages on the examined specimen. In addition, other applications of

this algorithm for ground tests / flights tests are being examined. The algorithm promises great potential in several fields of health and usage monitoring.

This study was presented in the the 58th Israel Annual Conference on Aerospace Sciences [22].

5.2 Towards a Physics Based Foundation for the Estimation of Bearings Remaining Useful Life (J. Bortman, BGU)

Rolling Element Bearing (REB) is one of the basic mechanical parts in rotating machines. Bearings are used to allow relative motion between the shaft and the housing under conditions of mutual loading. Since bearings are widely used, their failure is a topic of great interest. One of the common causes of REB failure is Rolling Contact Fatigue (RCF). Cyclic rolling contact with the rolling element (ball, cylinder, etc.) produces local damage that accumulates in the raceway of the bearing, initiating microcracks. The growth and coalescence of multiple microcracks form a longer crack that propagates toward the surface. Once the crack reaches the surface, a spall is generated. Generally, the existing bearing life models relate to the time or load cycles required for a small spall formation and do not describe the subsequent damage propagation process. However, after the first spall formation, the bearing might be fully operational for more than millions of cycles. Therefore, it is important to understand not only the damage initiation process, i.e. spall generation, but also the damage propagation, i.e. spall growth.

This study presents a concise introduction and description of a finite element (FE) based model for the analysis of the spall generation during the RCF process, with an emphasis on the microstructure and the damage evolution in the material. An example of this FEM is shown in Figure 26. It suggests a method for the damage initiation model assembly, towards a realistic representation of the grain topology and microscopic failure, using standard FE software tools.

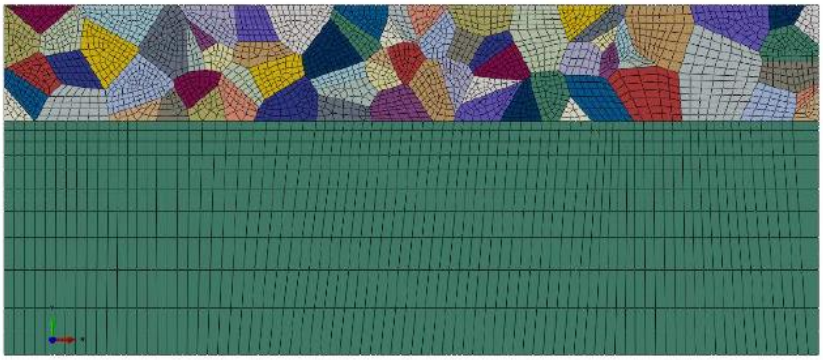

Figure 26. FEM with the microstructure representation at the near-surface region. Each color represents a different Young's Modulus.

By using the proposed method, the fatigue life of the REBs are calculated and analyzed using a two-parameter Weibull distribution function. Furthermore, the micro-cracks formation and spall generation are simulated. The results of the damage initiation model show a good agreement with previously published data, as shown in Figure 27.

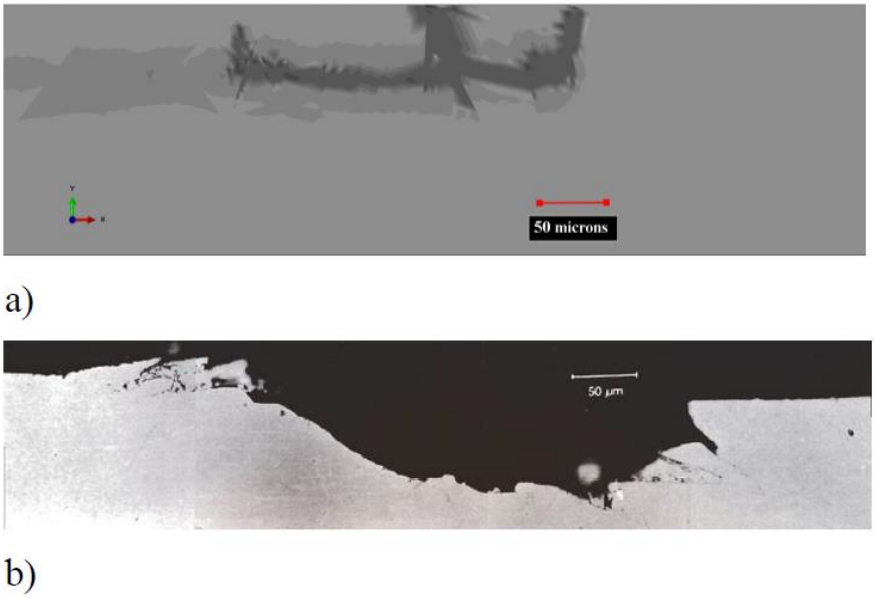

Figure 27. (a) Spall pattern received from one of the RCF simulations and (b) a section of the spall observed in experimental analysis

Prediction of the damage propagation in the REB, after the first spall generation, is not an easy task. The difficulties in prognosis of the propagation stage necessitate the deep understanding of the damage mechanisms, the stochastic nature of the spall propagation process, and its modeling. Figure 28 presents a roadmap for future research to develop a physics-based prognostic method for the spall propagation in the REB. The development of the method depends on the implementation of the research objectives and suggested methodology that are described and discussed in the full length paper [24].

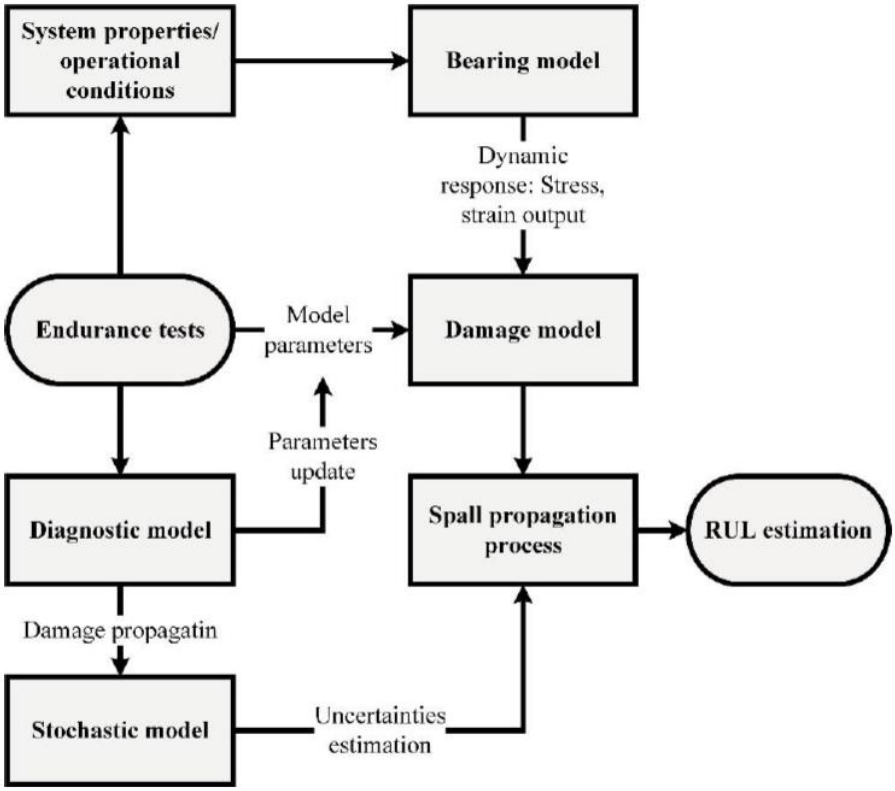

Figure 28. Research flow chart describing the steps toward the development of the RUL model

5.3 A Condition Based Maintenance Concept for Monitoring Helicopter Composite Rotor Blades (S. Shienkman, IAF, I. Kressel, IAI)

Helicopter rotor blades are elements that hold one of the most important structural roles in the rotorcraft. Providing thrust, lift and the ability to maneuver, the long beam-like aerodynamic structures undergo different dynamic loads at harsh environmental conditions. These high loads are reflected in complicated design criteria that eventually cause the burden of a strict and expensive maintenance policy that affects the platform's availability. This makes Condition Based Maintenance (CBM) a very attractive strategy for this component. CBM is the strategy of adapting an adequate maintenance policy based on a component's actual operation to improve availability and reduce maintenance cost. Many CBM systems implement their vision by continuously monitoring component's state of integrity. There is a variety of monitoring methods; each collects different parameters that produce more information about the material's current condition. These parameters can be processed to indicate global or local degradation of component properties, crack propagation, a beginning of a delamination, impact damage, matrix cracks and blade unbalance. As defects propagation in blades occur at very high rates only real-time diagnostic can prevent a catastrophe. Therefore, today's maintenance procedures which are performed on the ground after the helicopter has landed are insufficient and a constant monitoring of local and global changes is necessary.

This study demonstrates how an optical fiber based sensor mesh can be implemented on a rotor blade's trailing edge to identify defects by real-time monitoring of strain signatures under static load conditions. A schematic illustration of the optic fiber installation is shown in Figure 29.

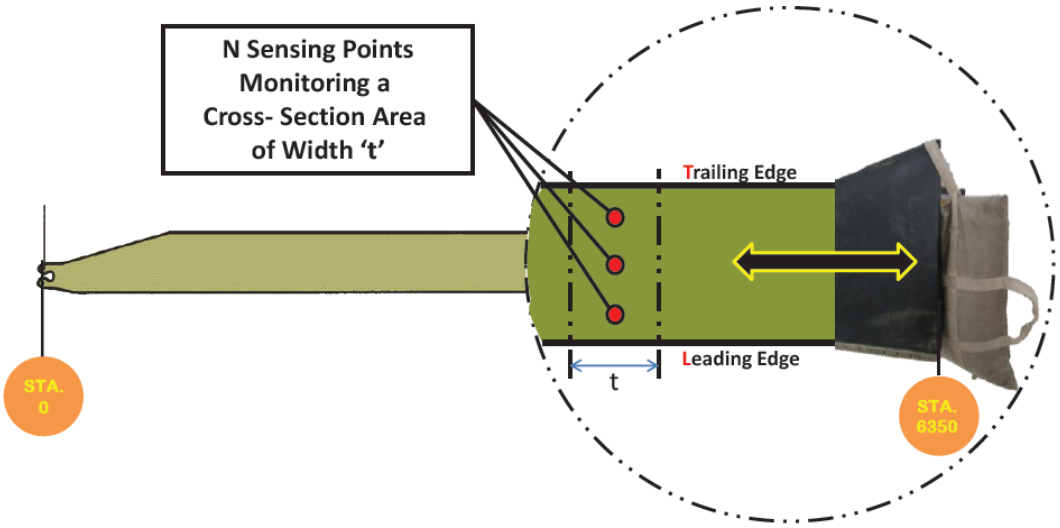

Figure 29. Schematic illustration of the monitoring concept in a Sikorsky S-76 main rotor blade.

Since no finite element model of the blade is available, two static experiments were performed, aiming to detect a critical defect size of about 2.5 [mm]. Both experiments were performed on a main rotor blade that is used in the IAF. The blade was cantilevered at its root on a droop. Each step of the experiment included loading the blade with increasing weight levels at its end, creating a growing moment at the tested point and recording the strain data. A crack-like defect was inserted at the testing point and the blade was again reloaded with the weight levels. The defect was propagated after every loading set. Figure 30 presents the test set-up.

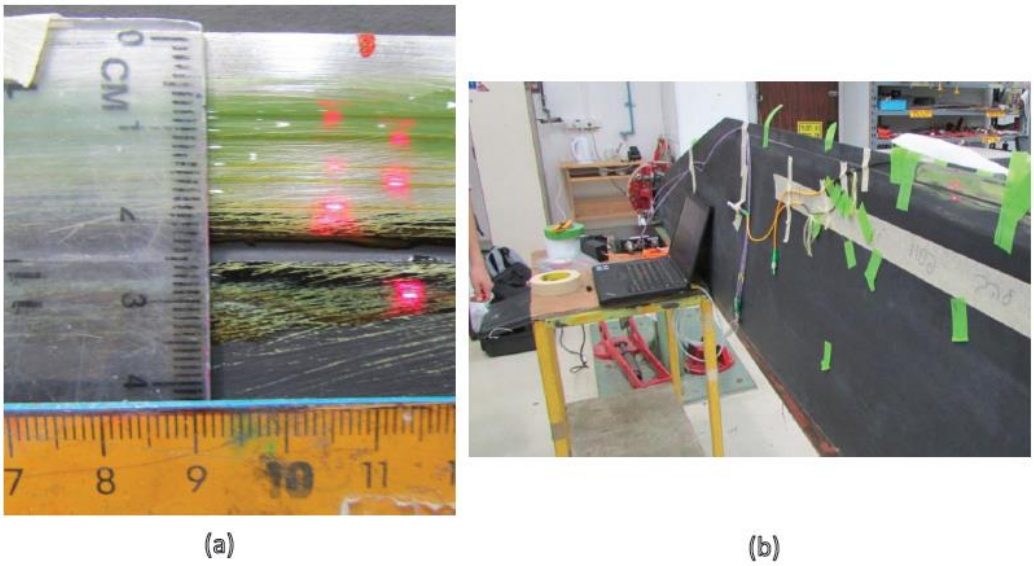

Figure 30. Sensor distribution (in red) and defect insertion location on the edge (a) and on the tested cantilevered blade (b)

In these tests a concept that can identify abnormal behavior due to the presence of a crack-like defect was demonstrated at a high level of confidence. It is expected that applying such a concept will improve availability of the helicopter by reducing down-time and maintenance cost. The full length paper includes further description of the test conducted, their results and the conclusions drawn from each test. It is given in Ref. [41].

5.4 Progress at BGU PHM Laboratory (J. Bortman, BGU)

The Ben Gurion University (BGU) Predictive Health Monitoring (PHM) laboratory research methodology for diagnostics and prognostics is physics-based. Each study process is based on physical models (kinematic and dynamic) and experiments with seeded faults. The methodology is based on understanding the physics of the machine components and their expression in the vibration signal in the presence of a fault. Prognostics techniques based solely on empirical data from experiments do not allow generalization of the results. Hence, change in the operating conditions of the monitored system can drastically change the vibration signature and make it difficult to estimate the component state. On the other hand, prognostics methods based solely on models do not guarantee compatibility with real systems. It is important to validate each model against a series of experiments in order to consolidate the physical assumptions and to ensure that the model simulates the reality well enough. Another requirement from the models is that the most important parameters should be considered in the modeling process to increase model credibility and to enable investigation of their influence. Modeling and experiments need to be combined to improve the research process and to reduce the disadvantages of each separate method.

Research Collaboration is a key factor for scientific breakthroughs and innovations. In 2018 a 3-years research collaboration has been established between the AFRL/RQTM Engine

Mechanical Systems Branch, located at Wright-Patterson AFB Ohio, USA and BGU PHM Laboratory, Israel. The goal of this collaboration is to improve vibration analysis, signal processing algorithms, and component failure detection methods for advanced bearing systems prognostic health monitoring (PHM) in a relevant engine environment.

Failure prognosis of the Rolling Element Bearings (REBs) is crucial in rotating machinery. The damage evolution in the REBs consists of two main phases: damage initiation and propagation. The conventional REB life models address the lifetime of the bearing to the damage initiation, i.e. first defect formation. An example of such model is provided in Ref. [51]. However, after the first defect formation, the bearing might be fully operational for millions of cycles. Over the past two decades, studies attempting to understand the damage mechanism and to develop damage propagation models have been published. Nevertheless, the damage mechanism is only partially understood, the existing models are inefficient and the physical phenomena are not well represented. In order to understand the spall propagation phase a physics-based model has been developed. A concise description regarding the model development is presented in Ref. [52]. The model aims to study the material behavior at the trailing edge of the spall during the Rolling Element (RE) impact. Based on the model results a qualitative damage analysis for crack evolution within the spall edge was conducted. Moreover, a metallurgical analysis of the bearing from endurance tests was carried out. The metallurgical analysis added insights regarding the damage mechanism and was used for model validation. The results achieved from the damage analysis are in good agreement with the experimental observations, Figure 31. This is the first study attempting to simulate damage evolution within the spall edge based on physical insight.

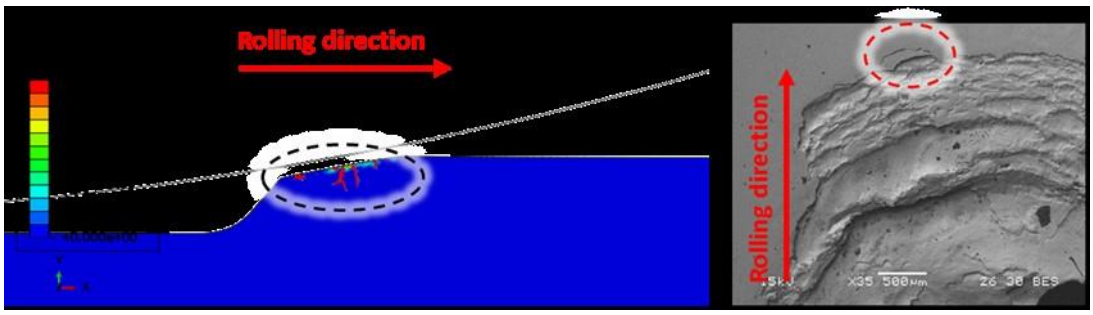

Figure 31. SEM images of the spall edge (right), FE model of the spall leading edge with simulated cracks (left)

A general dynamic model for rolling element bearings with and without a fault, based on the classic dynamic and kinematic equations, was developed [53]. Based on the general dynamic model, a deep understanding of the dynamics of a faulted bearing with a spalled race was obtained [54, 55]. A method for estimation of the spall size in bearing races was developed based on the physical understandings. First, the energy level and the rate at which the energy level changes as the fault grows was investigated [53]. It was found that the energy levels depended on the transmission function. Hence, the energy level differs for different systems, measurement locations, and operation conditions which make it difficult to use it for fault severity estimation. During examination of the simulation results, spall size estimation based

on the events which occur during the RE–spall interaction was proposed, Figure 32. The nature and sequence of events related to this interaction were used as the basis for the spall size estimation. Although several events occur during the interaction, the main ones are the entrance and the exit of the RE from the spall. A new event was discovered for the case of the spalled inner race – the collision between the RE and the outer race [54]. Discovering the new event had a significant effect on the ability to estimate the spall size. In a measured signal, the RE–outer race collisions concealed the exit event due to the transmission function effect on the signal. Hence, the exit moment can be estimated by the start of the impulse response decay.

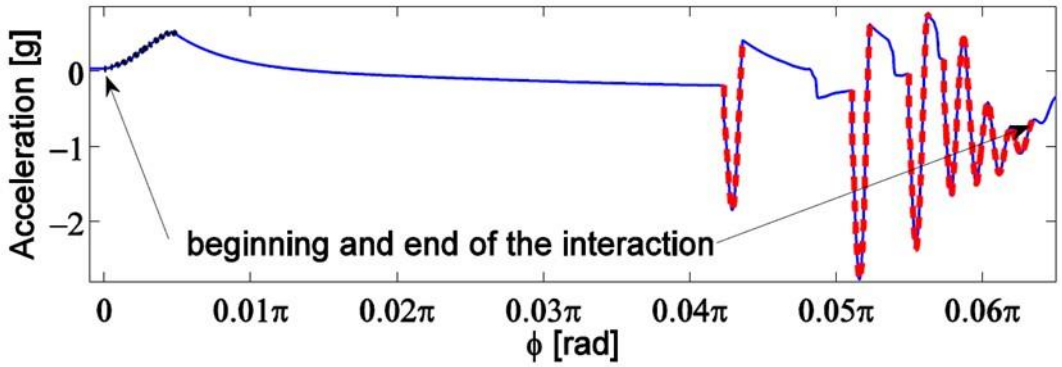

Figure 32. The simulated acceleration of the outer race. Spall in the outer race: solid blue line – simulated signal; dotted black line – RE-entrance edge contact; dashed red lines – RE–exit edge contacts

The effect of different parameters on the RE–spall interaction was investigated as well. It appears that the azimuth angle in which the interaction occurs has a substantial effect on the time between the main events. Explicit relations between this time and the spall size have been developed [56,57]. These insights and explicit relations allow the development of an algorithm [58] for spall size estimation that is based on two analytical models for the RE–spall interaction (for the inner and outer race cases). The analytical models produce explicit expressions which compute the necessary parameters for the algorithm. The principal parameters are the filter frequencies which are used to locate the main events and the explicit relations for the spall size. Different spall sizes located in the outer and inner races were estimated using the algorithm, which showed a good estimation capability [59].

One of the common methods for monitoring the health of REBs is through vibrations analysis. Our research examines a new method for monitoring rotating dynamic systems. In the new method, rather than measuring global vibrations, monitoring is performed by recording the local strains using optical Fiber Bragg Grating (FBG) sensors. This sensor has many advantages over a standard accelerometer. It can be mounted close to the monitored bearing due to its small dimensions and flexibility. The proximity of the sensor to the bearing reduces the effect of the transmission path and improves the signal-to-noise ratio. These sensors are not influenced by electromagnetic interference and do not generate such interference themselves. In addition, it is possible to put several sensors on a single fiber. Moreover, FBG sensors facilitate the detection of defects in REBs using simplified signal processing schemes and emphasizing the effects of the defect in the signal. Previous studies

have shown that FBG sensors can not only detect artificially implanted defects in REBs but their readings can be also processed to determine the size and severity of the defects. Several endurance tests were conducted. The goal of these tests was to identify and monitor the initiation and propagation of natural defects in the REBs. By using FBG sensors, we were able to continuously monitor the severity of the defect in the bearings and estimated the defect size at different stages of the experiment with less than 10% error, Figure 33.

.

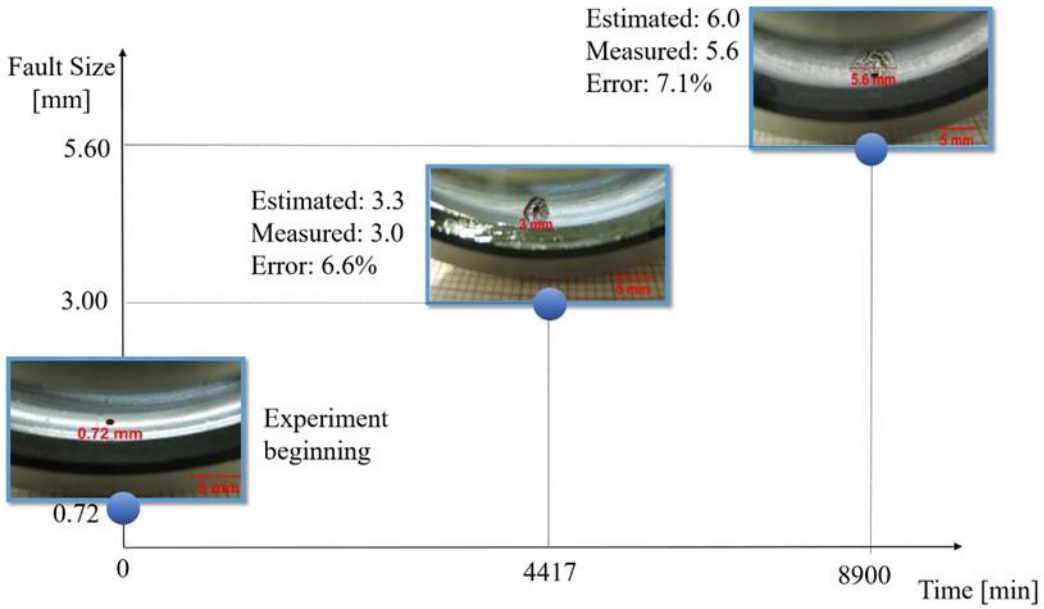

Figure 33. Validation of the fault size estimation during the endurance test.

Recently a new study on the Apache helicopter intermediate gearbox was launched. A unique test rig was completed to enable in-house research, and two experiments took place. An examination of the vibrations signature of the gearbox was conducted which aimed to distinguish between fully lubricated and under lubricated transmissions, and between transmission with normal and excessive backlash. Under-lubrication caused an increase in the vibration level and temperature. The backlash presented a change in vibrations that varied between the three axes. This phenomenon is due to the change in the pressure angle. An article detailing the experiments was published and presented in MFPT 2018 conference [60]. Furthermore, the existent spur gear model which is used in the laboratory was upgrade to simulate helical gears as well. The upgrade was accompanied by an experiment on a helical gear set to validate the model results.

Another research in the lab focuses on SHM aspects of Double Cardan shafts. Double Cardan shafts are common mechanisms for transmitting motion between non-collinear shafts. Although essential for various industrial applications, vehicles and marine vessels, cardan shafts monitoring is lacking and diagnostics can significantly improve. In order to understand the vibration analysis of a double Cardan shaft a kinematic analysis was carried out [61]. The model was compared to the vibrations measured on an experimental kit with real size cardan shaft,

Figure **34**. Analysis results illustrate the behavior of each component in the signature and comparison to experimental results taken on a real size cardan shaft confirms our understanding of the signal, Figure 35.

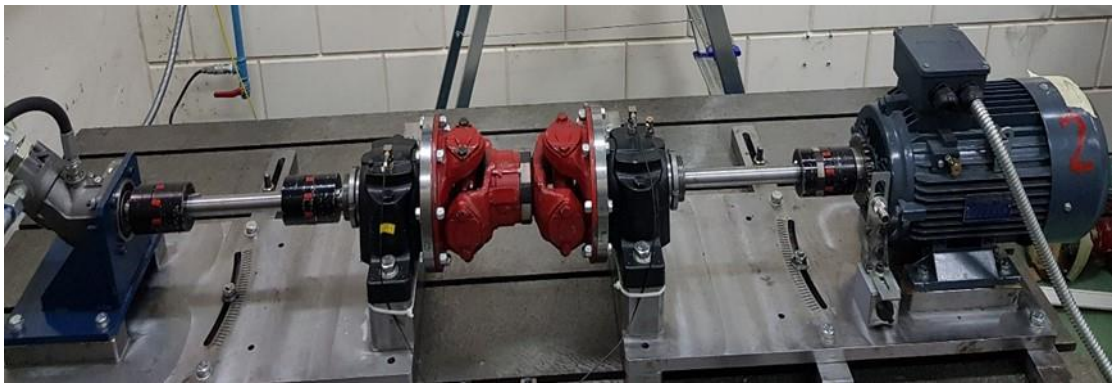

Figure 34. The Dounle cardan shaft kit

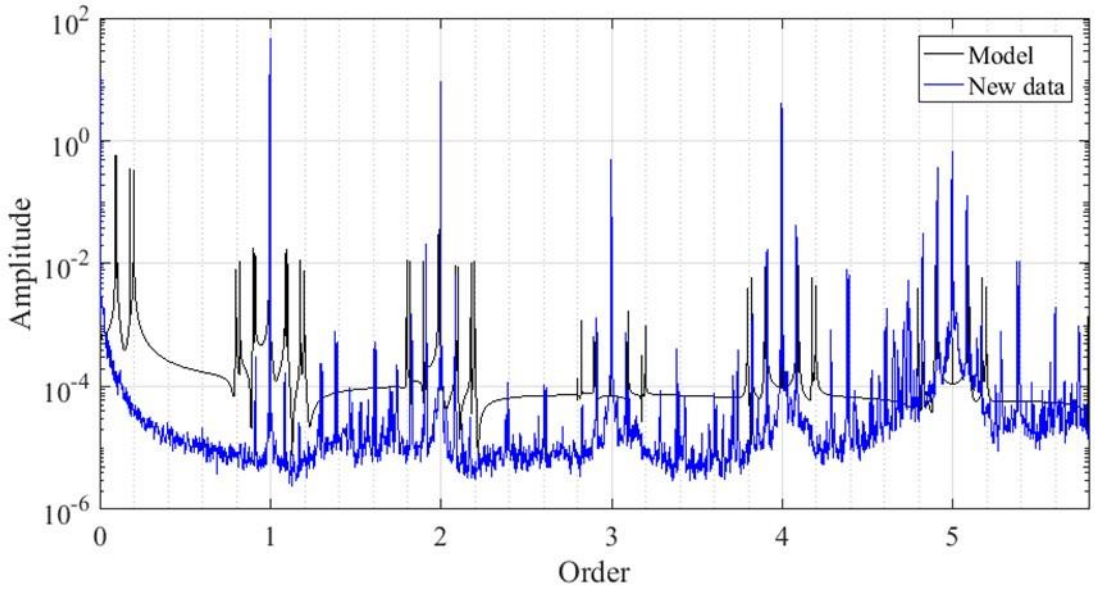

Figure 35. Experimental and simulated results of a double cardan shaft.

6. MISCELLANEOUS

6.1 New Book – "Stochastic Crack Propagation, Essential Practical Aspects" (G. Maymon, RAFAEL)

A new book on stochastic crack propagation was published on January 2018. This book summarizes practical aspects of stochastic crack propagation, many of them reported in previous National Reviews. Stochastic crack propagation introduces stochastic behavior to the procedures used for designing against fatigue phenomena in many products and structures. This aspect of the design process is not covered outside primary literature, but introducing the stochastic behavior of crack growth to the analysis and design procedures allows engineers to optimize for reliability. Each chapter in the book describes a feature important to the analysis of stochastic crack propagation, starting with the essential background theory. Processes or phenomena, which are of practical importance in the work of design engineers or R&D teams, are described chapter by chapter. Many examples are described and supported by listed references and files of data that can be used with specialist software to practice design situations. Advice on how to use various computer programs to design and predict for stochastic crack growth is included providing a complete guide for engineers and academics.

Dr. Giora Maymon obtained his Doctor of Sciences from Technion Israel Institute of Technology, 1975. He started work in RAFAEL – Armament Development Authority in 1963, so he has more than 50 years of experience in practical, project-oriented design. Dr. Maymon's work was centered on structural analysis and testing, structural dynamics, probabilistic structural analysis, and stochastic crack propagation. He is the author of two books and a participant in another two edited books, as well as having published numerous papers in the professional literature, and been an active participant in numerous scientific conferences. Additionally, he has more than 20 years of experience in stochastic crack propagation and wrote numerous RAFAEL internal reports on the subject.

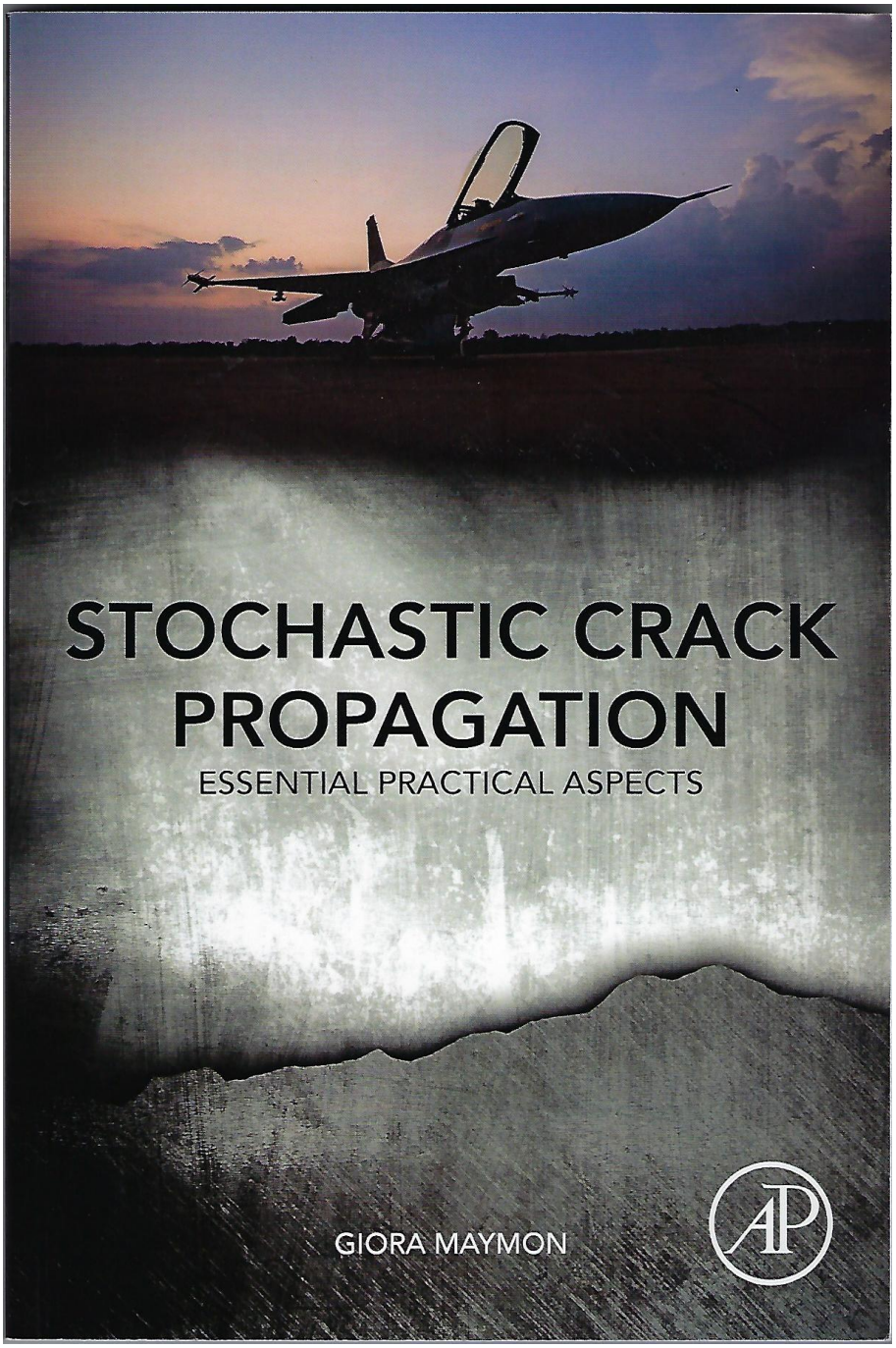

Figure 36. The cover of "Stochastic Crack Propagation, Essential Practical Aspects" book by Dr. Giora Maymon.

6.2 New Book – "Interface Fracture and Delaminations in Composite Materials" (L. Banks-Sills, TAU)

A new book was published in 2018 focusing on the subject of interface fracture between two linear elastic, homogeneous and isotropic materials, as well as between two dissimilar anisotropic materials [68]. The latter may be used to model the behavior of a delamination between two anisotropic plies. The Chapters include:

(1) Introduction
(2) Fundamentals of interface fracture mechanics
(3) Calculation of stress intensity factors - an interface crack
(4) Testing - interface crack between two isotropic materials
(5) Mathematical treatment of delaminations
(6) Methods of calculating stress intensity factors – delaminations
(7) Testing - delamination between two dissimilar plies

The book is based on years of investigation of interface cracks and delaminations with a host of students.

Professor Leslie Banks-Sills held the Diane and Arthur Belfer Chair of Mechanics and Biomechanics at Tel Aviv University from November 2006 until her retirement recently. She serves on the editorial boards of Engineering Fracture Mechanics, International Journal of Fracture, International Journal of Structural Integrity and Strain. She has consulted for various organizations in Israel, as well as for NASA, regarding problems of fracture in structures.

Professor Banks-Sills completed a B.A. degree in mathematics at Queens College of the City University of New York in 1965, an M.Sc. degree in engineering mechanics from the University of Michigan in 1973 and a Ph.D. degree in engineering from Harvard University in 1977. After carrying out a post-doctorate at Brown University, she joined the Faculty of Engineering at Tel Aviv University in 1979. From 1993 through 1997, and again from 2001 through 2005, she served as Chairman of the Department of Mechanics, Materials and Structures. She is Director of the Dreszer Fracture Mechanics Laboratory at Tel Aviv University.

She was a visiting scientist at Wright Patterson Air Force Base in the U.S. and the Research Center in Karlsruhe, Germany. The prestigious Mary Shepard B. Upson Visiting Professorship at Cornell University was awarded to her in 1997. Since 2001, she is an Adjunct Professor in the School of Civil and Environmental Engineering at Cornell University. She held the Lise Meitner Chair at Lund University, Sweden, from July, 2006 until December, 2006. In 2009, she was a Guest Professor in the Division of Solid Mechanics at Lund University. She was a Fellow of the Japan Society for the Promotion of Science at Kyoto University in 2009-2010. During her long career she won several prestige awards, such as the Hanin Prize for her contributions to aeronautical engineering in 2006, and the 2006 Honorary Membership to ESIS (European Society of Structural Integrity)

for her outstanding original technical contributions to fracture mechanics and good service to the international fracture mechanics community.

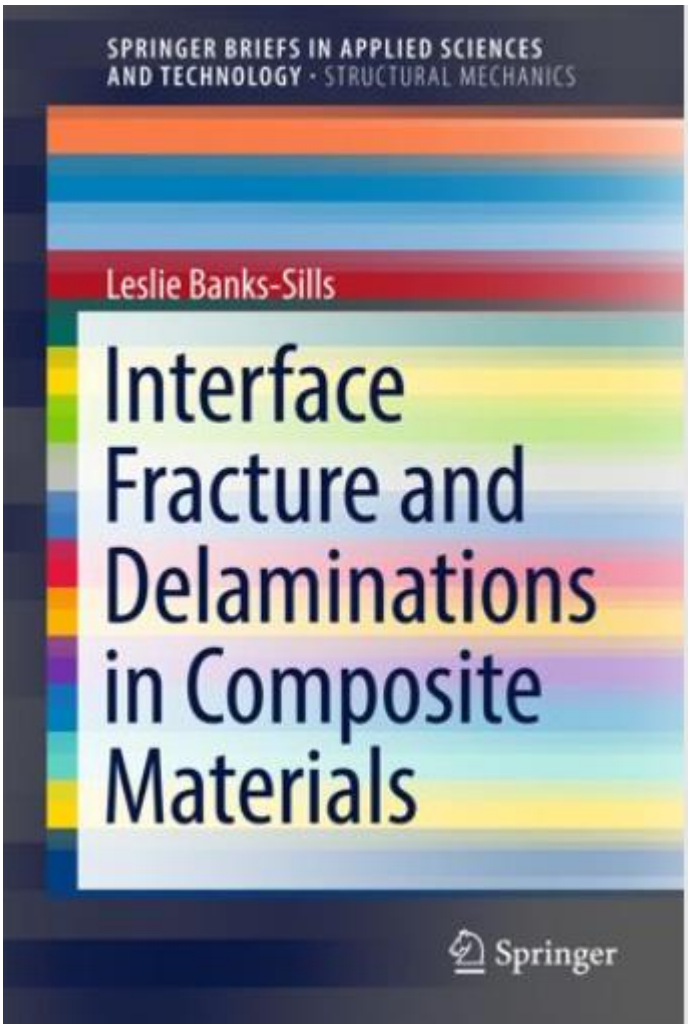

Figure 37. The cover of "Interface Fracture and Delaminations in Composite Materials" book by Prof. Leslie Banks-Sills.

6.3 Additive Layer Manufacturing Progress at IAI (E. Eigenberg, IAI)

IAI has been involved through the last fifteen years in many Additive Manufacturing(AM) national and international projects. Different disciplines, materials and methodologies were studied and developed during this period. IAI has many plastic AM machines which are able to manufacture different thermoplastic parts for mockups, tools, prototyping and for aircraft different applications. IAI also has a Markforged machine for composite R&D purposes. Two SLM Solutions machines for metallic parts have been used for the last 2-3 years for R&D and for structural applications in a number of running projects.

AM of Ti6Al4V alloy has been deeply investigated for structural applications during the last five years. Between years 2014-2015, IAI was the team leader of the 3D Printing work-package of the EU Clean-sky I Eco-design project in which almost all the aspects of the PB-AM technology and it accompanying disciplines were investigated. From topology optimization through detailed design to manufacturing and post processing. The demonstrator specimens were manufactured by an Electron Beam AM ARCAM machine, then HIP post processed to improve the internal discontinuities, MMP post processed to achieve the design surface roughness requirements and finally machined at the interface zones. Two specimens were tested according to the design fatigue spectrum at IAI ground test facilities. The test specimens performed poorly upon cyclic loads, but very important conclusions were drawn from this activity and were implemented in follow-on R&D projects. The test specimen and test fixture are shown below.

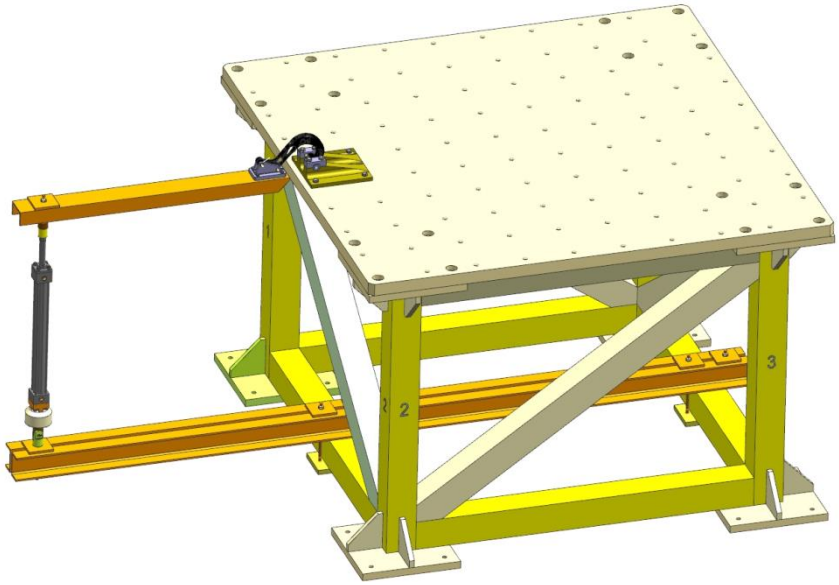

Figure 38. Clean Sky I Design of Demonstrator Test Fixture

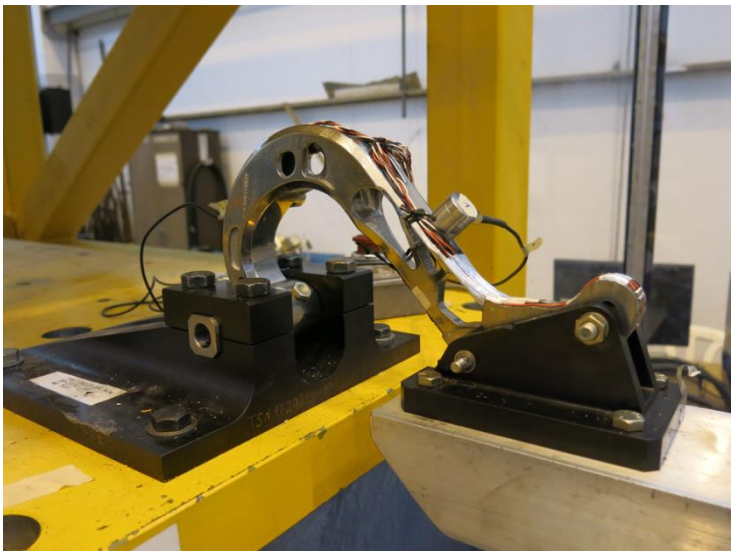

Figure 39. Clean Sky I Specimen Demonstrator Attached to the Test Fixture

To overcome the challenges identified in the CleanSky I project, IAI launched an in-house project aiming on improvement of the part design by reducing even more the mass of the optimized part and also by implementing the conclusions of the previous research. Four specimens were printed and again, two of them were tested according to the design fatigue spectrum at IAI ground test facilities. The two specimens endured more than ten times the previous two, withstanding more than one life cycle but yet without satisfying the design requirements. The root cause for the (still) early failure was investigated and it was found that the delivered parts by the subcontractor did not meet the surface roughness requirements defined in the drawing and in particular at the failure area. This test specimen is shown in Figure 40.

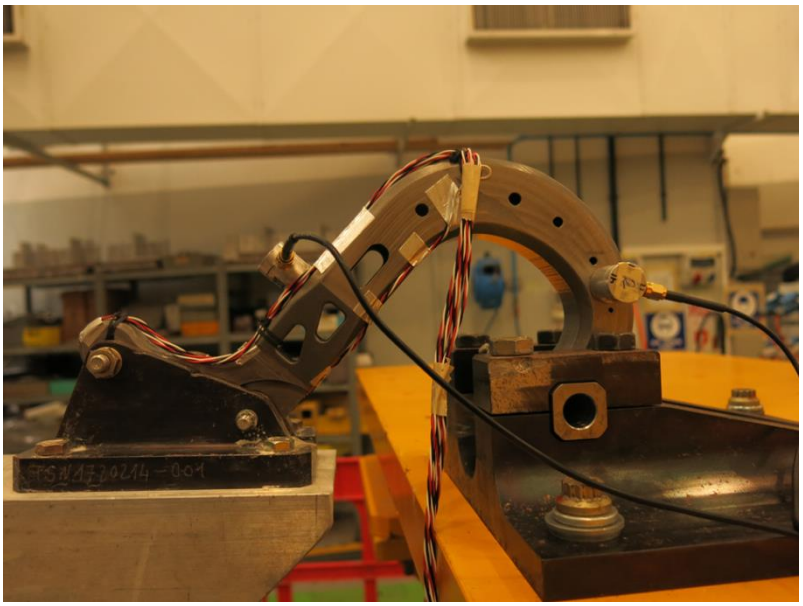

Figure 40. IAI improved Specimen Demonstrator Attached to the Test Fixture

During the last four years, IAI has been involved as a leading partner and as a design authority in a large R&D consortium for AM technologies financed by the Israeli Ministry of Economy named the "AATID" consortium. The goal of the project was to develop advanced design methodologies of optimized aero-structures made of Ti6Al4V alloy by additive manufacturing technologies. Three AM machines, which two of them are located at the Israel Institute of Metals (IIM) were used for this project. The first machine, located at the IIM was an EBM ARCAM-Q10 with a vast previous use by the experienced IIM team. The second machine was a new EOS-M290 ALM purchased by the Israel Ministry of Economy. The third machine was purchased by "Kanfit 3D", one of the R&D partners and located at their facilities. Also, a powerful micro-CT NDI equipment was purchased and placed at the AFEKA college facilities of the materials and processes center. Hundreds if not thousands of coupon samples were manufactured by these machines, by both of technologies. Design and optimization methodologies were developed. New and revolutionary fail safe concept was designed improving the robustness of the design and its endurance, all while reducing the original part weight. Printing parameters, the number of powder cycles re-use and their

impacts on the mechanical behavior were widely investigated for LBM and EBM technologies. Design allowable values for "HIPed" and machined PB-AM of Ti6Al4V alloy were set for the conventional static strength, for RT, ET and CT for each technology. S-N curves for R=0.1, R=-1.0, K_t = 1.0 and K=2.84 were obtained for each technology and the "B" basis curve for each of the eight curves was set. An Atlas from microstructures and from fractographic photos and studies was generated from the multiple results of the project to facilitate the engineering comprehension and judgment in future use. A special post-processing for the surface roughness improvement which is able to deal with the complexity and non-conventional nature of the optimized design structures was developed. From the results of the static and fatigue tests that were conducted at the IAI facilities it was concluded that all the different aspects and stages of the project, from the design until the final post-processing were a great success. The demonstrator of the "Aatid" consortium is shown in Figure 41 and Figure 42.

Figure 41. "Aatid" Consortium Specimen Demonstrator

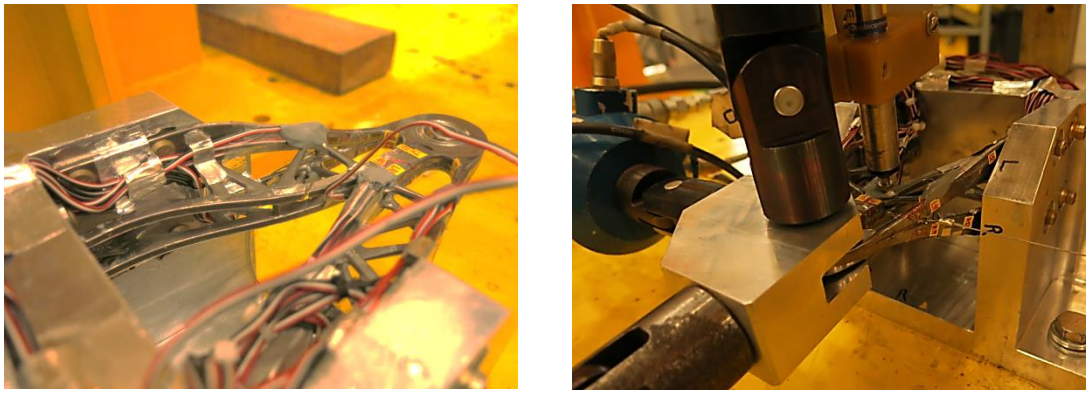

Figure 42. "Aatid" Consortium Specimen Demonstrator Attached to the Test Fixture

6.4 Progress at the Dreszer Fracture Mechanics Laboratory at Tel Aviv University (L. Banks-Sills, TAU)

During 2017 and 2018, The main area of interest at Tel Aviv University Dreszer Fracture Mechanics Laboratory has been characterization of the behavior of delaminations between plies of carbon fiber reinforced, laminate composite material. Two papers on two different material systems have investigated the nearly mode I deformation of a delamination in a multi-directional double cantilever beam (DCB) specimen [69, 70]. One laminate was fabricated from a prepreg and the second by means of a wet-layup process. For the prepreg, the delamination was between two plain woven plies with tows in the 0/90 (upper ply) and +45/-45 -directions (lower ply). For the wet-layup, the delamination was between a unidirectional (UD) fabric with fibers in the 0-direction and a plain woven ply with tows in the +45/-45 -directions. In both cases, a fracture resistance curve was obtained and fatigue delamination propagation were considered. Examples of the obtained R-curves is shown in Figure 43. The initial fracture toughness of the prepreg was about 30% higher than that of the wet-layup. The steady state values were quite close.

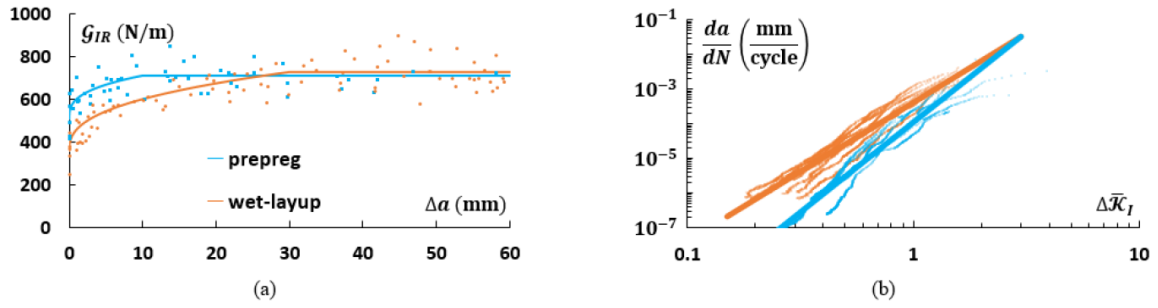

Figure 43. (a) Fracture resistance curves for prepreg and wet-layup. (b) Delamination propagation rate as a function of ΔK_I.

Next, fatigue delamination tests were carried out with the DCB specimens. For the prepreg, the cyclic displacement ratios were 0.1, 0.33, 0.5 and 0.75; for the wet-layup, there were 0.1 and 0.48. The delamination propagation rate da=dN is plotted with respect to various functions of the energy release rate, with

$$\hat{\mathcal{G}}_{Imax} = \frac{\mathcal{G}_{Imax}}{\mathcal{G}_{IR}} \ .$$

Note that $\mathcal{G}_{Imax}$ is the maximum value of $\mathcal{G}_I$ in a cycle and $\mathcal{G}_{IR}$ is the value of the energy release rate from the resistance curve. A second parameter which has been used to plot fatigue data is

$$\Delta\hat{\mathcal{G}}_{Ieff} = \left(\sqrt{\hat{\mathcal{G}}_{Imax}} - \sqrt{\hat{\mathcal{G}}_{Imin}}\right)^2 \ .$$

For both of these parameters, the full fatigue delamination curves may be found as that shown in Figure 44. It may be observed that all g_{Imax} curves approach the critical energy release rate for high values of da-dN but different threshold values, for small values of da-dN. On the other hand, if the fatigue data is plotted using g_{Ieff}, different critical value is reached for high values of da-dN, whereas one threshold value is reached for all ratios. This fact is used to determine g_{Ithr}.

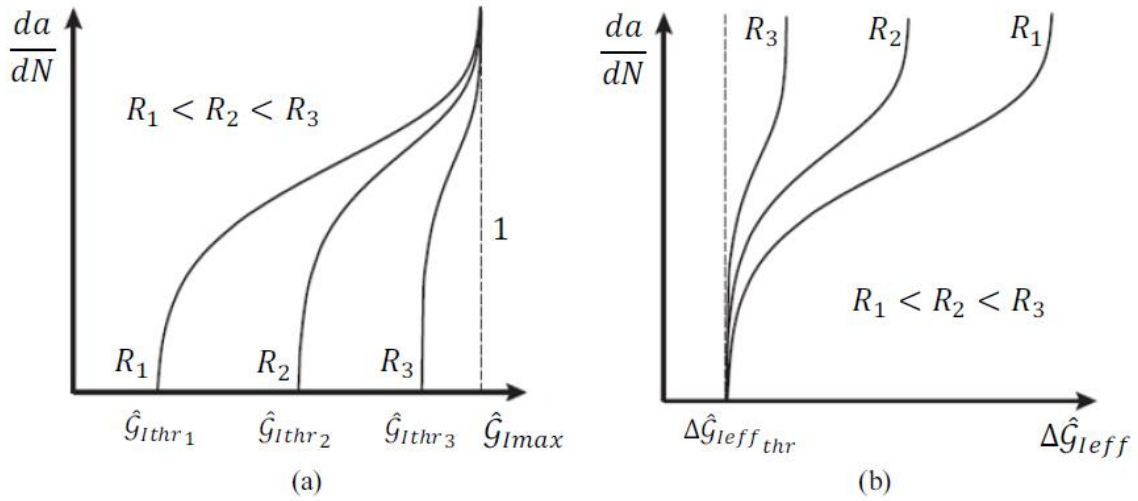

Figure 44. Schematic description of fatigue test data for different cycle ratios on a log-log scale. da-dN vs. (a) g_{Imax} and (b) g_{Ieff}

A third parameter used to plot fatigue data is

$$\Delta\bar{\mathcal{K}}_I = \frac{\sqrt{\hat{\mathcal{G}}_{Imax}} - \sqrt{\hat{\mathcal{G}}_{Ithr}}}{\sqrt{1 - \sqrt{\hat{\mathcal{G}}_{Imax}}}}$$

which is based on the Hartman-Schijve [71] equation for metals. The threshold values for both material systems and cyclic load ratios are found in [69] and [70]. Using this parameter, it is possible to obtain a master-curve for each material system, as shown in Figure 43b. In this figure, the dots are the data from the fatigue delamination propagation tests, while the solid lines are the master-curves for each material system. The master-curves provide a full description of fatigue delamination propagation for each material system without dependence on the cycle ratio. The slope of the Paris type equation for the wet-layup was lower than that of the prepreg. But the fatigue delamination propagation rate was lower for the latter.

Several presentations [72-75] on the prepreg were given summarizing these results. Tomer Chocron completed an M.Sc. degree on the nearly mode I fracture and fatigue behavior of the

wet-layup [76]. After characterizing the material in nearly mode I deformation, modes II and mixed mode deformation should be investigated. To this end, for the same interfaces and fabrication processes, Brazilian disk specimens were manufactured as shown in Figure 45. By changing the loading angle, this specimen produces various ratios of in-plane mixed mode deformation. The load and crack or delamination length at fracture were measured and used in a finite element analysis to determine the displacement field. An interaction energy or M-integral was used to determine the stress intensity factors at failure. These in turn were employed to obtain the critical interface energy release rate, and two phase angles which measure the mode mixity. Two Ph.D. students have carried out tests on these specimens. For the wet-layup, two presentations were made at conferences [77, 78]. For the latter, a conference paper was published. In addition, an invitation to deliver the ASTM Swedlow Memorial Lecture was extended [79]. The presentation dealt with obtaining a statistically based failure curve or surface for mixed mode deformation of interface cracks and delaminations in laminates. All of this work was based on tests with Brazilian disk specimens.

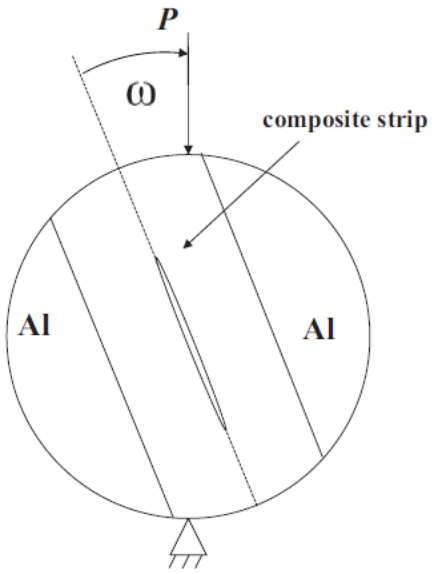

Figure 45. Brazilian disk specimen composed of a central composite strip within two aluminum partial disks.

Studies are continuing on the Virtual Crack Closure Technique (VCCT). This method was first presented in Ref. [80] for cracks in linear elastic, homogeneous and isotropic material with four noded elements. It makes use of the Irwin crack closure integral to obtain values of the modes I, II and III energy release rates from finite element data. The method was extended to eight noded and quarter-point elements. It may easily be extended to anisotropic material. In addition, it was extended to cracks along an interface between two dissimilar linear elastic, homogeneous and isotropic materials. In that case, the energy release rates were seen to depend upon the size of the virtual crack extension usually taken as the size of the element adjacent to the crack tip. Some attempts have been made to remove this dependence.

Nevertheless, in most cases, the accuracy of both the energy release rates and stress intensity factors was not consistently good.

In Ref. [81], the dependence of the energy release rates on the size of the virtual crack extension for interface cracks was analytically accounted for so that the stress intensity factors may be accurately obtained when fine finite element meshes are used, together with a virtual crack extension consisting of more than one element. In Ref. [82], the equations for an interface crack between two dissimilar linear elastic, homogeneous and transversely isotropic materials were derived. Dual energy release rates were defined which enabled choice of an optimal number of elements to be included in the virtual crack extension. In addition, in previous papers, use of elements smaller than the interpenetration zone were rejected. In this study, it was shown that these elements may, indeed, be used. Moreover, it was shown that by using focused meshes, it is possible to reduce substantially the number of elements used in the calculations.

Most recently, the VCCT was derived once more. The new derivations allow for a better understanding of this method showing that quarter-point (QP) elements are not appropriate for VCCT. It may be observed in Fig. 5 that the quarter-point nodal points do not have the same relative location in the element in which nodal point forces are calculated and in the element where displacement jumps are calculated. Various options for dealing with this problem have been examined. Careful consideration of finite element analyses confirms that eight-noded regular elements are preferred. By means of both analytical and numerical calculations, a criterion for determining the length of the virtual crack extension using the dual energy release rates was examined. In addition, for an interface crack, a new and more suitable equation for calculating the phase angle of the complex stress intensity factor was presented. A manuscript has been written based on these findings and submitted for publication [83].

5 REFERENCES

1. Freed Y., "Review of Aeronautical Fatigue Investigations in Israel, January 2015 – December 2016", *Minutes of the 35rd ICAF Conference*, Nagoya, Japan, 2017.

2. Freed Y., "Implementation of invariant-based for determination of composite materials allowables", *56th Israel Annual conference on Aerospace Sciences*, 2016, Tel Aviv, Israel.

3. Goose J.H. and Christensen S., "Strain Invariant Failure Criteria for polymers in Composite Materials", AIAA-2001/1184, 2001.

4. Tay T.E. et al., "Damage Progression by the Element-Failure Method (EFM) and the Strain Invariant Theory (SIFT)", *Composite Science and Technology*, 65, 2005.

5. Aboudi J., "The Generalized Method of Cells and High-Fidelity Generalized Method of Cells Micromechanical Models – A Review", *Mechanics of Advanced Materials and Structures*, 11, 2004.

6. Stanley J. et al., "SIFT analysis of IM7/5250-4 composites", *36th ISTC Conference*, San Diego, California, 2004.

7. Tsai S.W., Strength & Life of Composites, *Composite Design Group*, Stanford University, USA, 2008.

8. Freed Y., "Implementation of a Micro-Mechanical Approach for Failure Predictions of Composite Materials", *58th Israel Annual Conference on Aerospace Sciences*, 2018, Tel Aviv, Israel.

9. Boerstra G.K., "The multislope model: a new description for the fatigue strength of glass reinforced plastic". *Int J Fatigue*, 2007, 29(8):1571-1576.

10. Harris. B, "A parametric constant-life model for prediction of the fatigue lives of fibre-reinforced plastics". In: Harris. B, editor. Fatigue in Composites. Woodhead Publishing Limited; 2003; p. 546-568

11. Philippidis, T.P., and Vassilopouloss, A.P., "Life prediction methodology for GFRP laminates under spectrum loading". *Composites: Part A*, 2004; 35(6):657-666.

12. Kawai M, Koizumi M. "Nonlinear constant fatigue life diagrams for carbon/epoxy laminates at room temperature". *Composites: Part A* 2007; 38(11):2342–53.

13. Kawai M, Teranuma T. "A multiaxial fatigue criterion based on the principal constant life diagrams for unidirectional carbon/epoxy laminates". *Composites: Part A* 2012;43(2012):1252-1266.

14. Buimovich Y. and Elmalich D., "Examination of the KAWAI CLD Method for Fatigue Life prediction of Composite Materials", *58th Israel Annual Conference on Aerospace Sciences*, 2018, Tel Aviv, Israel.

15. Tsai, S.W., Wu, E.M., "A General Theory of Strength for Anisotropic Materials", *Journal of Composite Materials* 5, 58-80, 1971.

16. Argon, A.S., "Fracture of Composites". in *Treatise on Materials Sciency and Technology*,Vol. 1, Herman, H. editor, Academic Press, pp. 79-114, 1972.

17. Budiansky, B., "Micromechanics", *Computers and Structures*, Vol. 16, pp.3-12, 1983.

18. Hahn, H.T.a.W., J. G., "Compression Failure Mechanisms in Unidirectional Composites", Composite Materials: Testing and Design (Seventh Conference), ASTM STP 893, Whitney, J., editor, American Society for Testing and Materials, pp. 115-139, 1986.

19. Lo, K.H., Chim, E.S.-M., "Compressive Strength of Unidirectional Composites", *Journal of Reinforced Plastics and Composites* 11, 838-896, 1992.

20. Rosen, B.W., "Mechanics of composite strengthening"., in Fiber Composite Materials, American Society for Metals, Metals Park, Ohio, pp. 37-75, 1965.

21. Massarwa E. et al., "A Multiscale Progressive Damage Analysis for Laminated Composite Structures using the Parametric HFGMC Micromechanics", Accepted for publication at Composite Structures, doi: https://doi.org/10.1016/j.compstruct.2017.11.089

22. Dorfman B. et al., "Characteristics Pattern Recognition Algorithm for Health and Usage Monitoring", *58th Israel Annual Conference on Aerospace Sciences*, 2018, Tel Aviv, Israel.

23. Breiman U at al., "Semianalytical Compressive Strength Criteria for Unidirectional Composites", *Journal of Reinforced Plastics and Composites*, 37, 2018.

24. Gazizulin D. et al., "Towards a Physics Based Foundation for the Estimation of Bearings RUL*", Asia Pacific Conference of the Prognostics and Health Management Society*, Jeju, Korea, July 2017.

25. Brot A., "The Dual Threat of Sudden Decompression", *58th Israel Annual Conference on Aerospace Sciences*, 2018, Tel Aviv, Israel.

26. Matias C. and Elmalich, D., "Influence of Finite Width Dimensions on Mutual Interaction of Two Opposing Cracks at a Hole", *58th Israel Annual Conference on Aerospace Sciences*, 2018, Tel Aviv, Israel.

27. Abernethy R.B., "The New Weibull Handbook", 5th edition, 2009.

28. Brot A., "Nearly Identical Twins or Distant Cousins, Revisited. Weibull or Log-Normal Distributions to Characterize Fatigue Life Scatter – Which is Recommended?", to be presented in *30th symposium of the International Committee on Aeronautical Fatigue and Structural Integrity*, Krakow, Poland, 2019.

29. Buimovich Y. and Elmalich D., "Examination of the KAWAI CLD Method for Fatigue Life Prediction of Composites", to be presented in *30th symposium of the International Committee on Aeronautical Fatigue and Structural Integrity*, Krakow, Poland, 2019.

30. Brot A., "Weibull or Log-Normal Distributions to Characterize Fatigue Life Scatter. Are we closer to a solution?", *59th Israel Annual Conference on Aerospace Sciences*, 2019, Tel Aviv, Israel.

31. Bathias C., "There is no infinite fatigue life in metallic materials", *Fatigue & Fracture of Engineering Materials & Structures* 07;22(7):559-65, 1999.

32. Kazymyrovych V., "Very high cycle fatigue of engineering materials (a literature review)", Karlstad University, 2009.

33. Wang Q., Khan M.K. and Bathias C., "Current Understanding of Ultra-High Cycle Fatigue", *Theoretical and Applied Mechanics Letters*, 2, 031002, 2012.

34. Murakami Y., "Metal Fatigue: Effects of Small Defects and Non-metallic Inclusions", Elsevier, 2002.

35. Metallic Materials Properties Development and Standardization (MMPDS), MMPDS-07, 2012.

36. Amos R.J., Whitelaw A. and Hussain M.A., "An Algorithm for the Prediction of Very High Cycle Fatigue Life", *Proceedings of the 28th ICAF Symposium*, Helsinki, 2015.

37. Sonsino C.M., "Course of SN-curves especially in the high-cycle fatigue regime with regard to component design and safety", *Int J Fatigue* 29:2246-58, 2007.

38. Safarian P., "Fatigue and damage tolerance advanced concept course", CAAI, Israel, 2014.

39. Buimovich Y. and Binyamin T., "Examination of Algorithms for Prediction of Very High Cycle Fatigue Life", *59th Israel Annual Conference on Aerospace Sciences*, 2019, Tel Aviv, Israel.

40. Matias C., Levi-Sasson A. and Katsav E., "Why Should We Encourage Usage of Interference-Fit Fasteners at Airframe Structural Joints", to be presented in *30th symposium of the International Committee on Aeronautical Fatigue and Structural Integrity*, Krakow, Poland, 2019.

41. Shienkman S., Farajun I., Ben-Simon U., Kressel I., Glam B. and Ishbir C., "A Condition Based Maintenance Concept for Monitoring Helicopter Composite Rotor Blades", *58th Israel Annual Conference on Aerospace Sciences*, 2018, Tel Aviv, Israel.

42. Hartman A. and Schijve J., "The effect of secondary bending on the fatigue strength of 2024-T3", NLR, Amsterdam, Technical Report 69116, 1969.

43. Schijve J., "Fatigue of structures and materials", Dordrechrt, The Netherlands, Springer, 2001.

44. De Rijck J.J.M, "Stress analysis of fatigue cracks in mechanically fastened joints. An analytical and experimental investigation", PhD Thesis, Delft University of Technology, 2005.

45. Schijve J., "Riveted lap joints with a staggered thickness in the overlap of the joint. Calculations of secondary bending", Faculty of Aerospace Engineering, Delft, 2006 [Doc. B2-06-02].

46. Shijve J. and Campoli G., "Fatigue of structures and secondary bending in structural elements", *International Journal of Fatigue*, DOI:10.1016/j.ijfatigue.2009.01.009.

47. Skorupa M. et al., "Observation and analyses of secondary bending for riveted lap joints", *International Journal of Fatigue* 72, p. 1-10, 2015.

48. Skorupa M. et al., "Fatigue strength reduction factors at rivet holes for aircraft fuselage lap joints", *International Journal of Fatigue* 80, p. 417-425, 2015.

49. Magidish O., Freed Y., Elmalich D., Mayo A. and Sagi Machnes L., "Numerical Investigation of the Effect of Secondary Bending in Hard-point Joints", 59th Israel Annual Conference on Aerospace Sciences, 2019, Tel Aviv, Israel.

50. Freed Y., Sagi Machnes L. and Magidish O., "Analytical and Numerical Investigation of the Effect of Secondary Bending in Hard-Point Joints", to be presented in 30th symposium of the International Committee on Aeronautical Fatigue and Structural Integrity, Krakow, Poland, 2019.

51. D. Gazizulin, R. Klein and J. Bortman, "Towards Efficient Spall Generation Simulation in a Rolling Element Bearing", Fatigue & Fracture of Engineering Materials & Structures, 2017, DOI: 10.1111/ffe.12580; IF 2.335; JCR, 32/130, Q1.

52. D. Gazizulin, R. Klein and J. Bortman, "Physics Based Methodology for the Estimation of Bearings' Remaining Useful Life: Physics-Based Models, Diagnostic Methods and Experiments", Fourth European Conference of the PHM Society 2018, Utrecht, Netherlands, 2018.

53. G. Kogan, R. Klein, A. Kushnirsky, J. Bortman, Toward a 3D dynamic model of a faulty duplex ball bearing, Mech. Syst. Signal Process. 54, 2015, p. 243–258. doi:10.1016/j.ymssp.2014.07.020.

54. E. Madar, G. Kogan, R. Klein, J. Bortman, Estimation of spall size in bearing inner race based on vibration analysis, in: Thirteen. Int. Conf. Cond. Monit. Mach. Fail. Prev. Technol., Paris, France, 2016.

55. G. Kogan, E. Madar, R. Klein, J. Bortman, Spall size estimation in bearing races based on vibration analysis, in: Annu. Conf. Eur. Conf. Progn. Heal. Manag. Soc., Bilbao, Spain, 2016.

56. G. Kogan, J. Bortman, R. Klein, A new model for spall-rolling-element interaction, Nonlinear Dyn. 87, p. 219–236, 2017. doi:10.1007/s11071-016-3037-1.

57. E. Madar, G. Kogan, R. Klein, J. Bortman, An analytical model for rolling-element-spall interaction in bearing inner race, in: First World Congr. Cond. Monit. Conf., London, England, 2017.

58. G. Kogan, R. Klein, J. Bortman, A Physics-Based Algorithm for the Estimation of Bearing Spall Width Using Vibrations, Mech. Syst. Signal Process. under Rev., 2017.

59. E. Madar, G. Kogan, D. Gazizulin, R. Klein, J. Bortman, Steps toward prognostics of faults in bearings, in: Ninth Conf. Progn. Heal. Manag. Soc., St. Petersburg, Florida, United States, 2017.

60. N. Silverman, I.Dadon, J. Bortman, A. Kushnirsky, D. Meron, and R. Klein, "The effect of grease level and backlash on the AH-64 intermediate gearbox using a unique test rig" NDT-MFPT conference, Nottingham, England, 2018.

61. M. Battat, R. Klein and J. Bortman, Vibration Analysis of a Double Cardan Shaft, The First World Congress on Condition Monitoring (WCCM 2017), London, England, 2017.

62. Perl, M., and Steiner, M., "The Beneficial Effect of Full or Partial Autofrettage on the Combined 3-D Stress Intensity Factors for Inner Radial Crack Arrays in a Spherical Pressure Vessel," Engineering Fracture Mechanics, 175, 2017, pp. 46-56.

63. Perl, M., and Saley, T., "Swage and Hydraulic Autofrettage Impact on Fracture Endurance and Fatigue Life of an Internally Cracked Smooth Gun Barrel Part I - The Effect of Overstraining," Engineering Fracture Mechanics, 182c, (2017), pp. 372-385.

64. Perl, M., and Saley, T., "Swage and Hydraulic Autofrettage Impact on Fracture Endurance and Fatigue Life of an Internally Cracked Smooth Gun Barrel Part II- The Combined Effect of Pressure and Overstraining," Engineering Fracture Mechanics, 182c, (2017), pp. 386-399.

65. Perry, J., and Perl, M., "The Effects of the Material's Exact Yield Point and its Plastic Properties on the Safe Maximum Pressure of Gun Barrels," Trans. of the ASME, Journal of Pressure Vessel Technology, 139, 5, 051401 (2017).

66. Perl, M., and Steiner, M., "The Beneficial Effect of Full or Partial Autofrettage on the Combined 3-D Stress Intensity Factors for Inner Coplanar Crack Arrays and Ring Cracks in a Spherical Pressure Vessel," Engineering Fracture Mechanics, 191, (2018), pp. 426-440.

67. Perry, J., and Perl, M., "Gun Barrel Refurbishing Using a Shrink-Fitted Autofrettaged Liner," Trans. of the ASME, Journal of Pressure Vessel Technology, 140, 2, 021203 (2018).

68. L. Banks-Sills, "Interface Fracture and Delaminations in Composite Material" Springer, Cham, Switzerland (2018).

69. I. Simon, L. Banks-Sills and V. Fourman, "Mode I delamination propagation and R-ratio effects in woven composite DCB specimens for a multi-directional layup", International Journal of Fatigue, 96 (2017) 237-251.

70. T. Chocron and L. Banks-Sills, "Nearly mode I fracture toughness and fatigue delamination propagation in a multi-directional laminate fabricated by a wet-layup", Fizicheskaya Mezomekhanika, (in Russain), 21 (2018) 103-134; Physical Mesomechanics, (in English), 22, (2019).

71. A. Hartman and J. Schijve, “The effects of environment and load frequency on the crack propagation law for macro fatigue crack growth in aluminium alloys”, Engineering Fracture Mechanics 1 (1970) 615-631.

72. L. Banks-Sills and I. Simon, “R-ratio effects on fatigue delamination propagation mode I”, Barentblatt Symposium (invited), International Congress on Fracture 14 (ICF14), Rhodes, Greece (2017).

73. I. Simon and L. Banks-Sills, “The effect of the Hartman-Schijve representation of fatigue delamination growth test data for CFRP on da-dN”, International Congress on Fracture 14 (ICF14), Rhodes, Greece (2017).

74. L. Banks-Sills and I. Simon, “Fatigue delamination propagation in a woven multi-directional composite in mode I”, (plenary) International Conference on Structural Integrity and Durability 2017 (ICSID 2017), Dubrovnik, Croatia (2017).

75. L. Banks-Sills and I. Simon, “Woven multi-directional composite: mode I fatigue delamination propagation”, (plenary) Greek Society for Experimental Mechanics of Materials, Athens, Greece (2018).

76. T. Chocron. “Delamination propagation in a multi-directional laminate composite DCB specimen produced by a wet-layup”, M.Sc., Tel Aviv University (2018).

77. L. Banks-Sills and M. Mega, “Mixed mode failure criterion for a multi-directional laminate”, International Conference on Experimental Mechanics 18 (ICEM18), Brussels, Belgium (2018).

78. M. Mega and L. Banks-Sills, “Testing of Brazilian disk specimens with a delamination between a transversely isotropic and a tetragonal composite ply”, Procedia Structural Integrity 13, 123-130, European Conference of Fracture (ECF22), 2018, Belgrade, Serbia.

79. L. Banks-Sills, “Statistical analysis for interface fracture and delamination failure of composites”, (Swedlow Memorial Lecture), ASTM 41st National Symposium on Fatigue and Fracture Mechanics, Toronto, Canada (2017).

80. E.F. Rybicki and M.F.Kanninen, “A finite element calculation of stress intensity factors by a modified crack closure integral”, Engineering Fracture Mechanics, 9 (1977) 931-938.

81. L. Banks-Sills and E. Farkash, “A note on the Virtual Crack Closure Technique for an interface crack”, International Journal of Fracture, 201 (2016) 171-180.

82. E. Farkash and L. Banks-Sills, “Virtual crack closure technique for an interface crack between two transversely isotropic materials”, International Journal of Fracture, 205 (2017), 189-202.

83. E. Farkash and L. Banks-Sills, “Quarter-point elements are unnecessary for the virtual crack closure technique”, Submitted for publication.